Molecular Therapy
Nucleic Acids
Original Article

Aptamer-Functionalized Drug Nanocarrier Improves Hepatocellular Carcinoma toward Normal by Targeting Neoplastic Hepatocytes

Samrat Chakraborty,[1] Zewdu Yilma Dlie,[1,6] Somdyuti Chakraborty,[1] Somdatta Roy,[1] Biswajit Mukherjee,[1] Shila Elizabeth Besra,[4] Saikat Dewanjee,[3] Alankar Mukherjee,[1] Probir Kumar Ojha,[2] Vinay Kumar,[2] and Ramkrishna Sen[1,5]

[1]Pharmaceutics Research Laboratory, Department of Pharmaceutical Technology, Jadavpur University, Kolkata, India; [2]Drug Theoretics and Cheminformatics Laboratory, Department of Pharmaceutical Technology, Jadavpur University, Kolkata, India; [3]Advanced Pharmacognosy Research Laboratory, Department of Pharmaceutical Technology, Jadavpur University, Kolkata, India; [4]Cancer Biology and Inflammatory Disorder Division, CSIR-Indian Institute of Chemical Biology, Kolkata, India; [5]Infectious Diseases and Immunology Division, CSIR-Indian Institute of Chemical Biology, Kolkata, India

Site-specific delivery of chemotherapeutics specifically to neoplastic hepatocytes without affecting normal hepatocytes should be a focus for potential therapeutic management of hepatocellular carcinoma (HCC). The aptamer TLS 9a with phosphorothioate backbone modifications (L5) has not been explored so far for preferential delivery of therapeutics in neoplastic hepatocytes to induce apoptosis. Thus, the objective of the present investigation was to compare the therapeutic potential of L5-functionalized drug nanocarrier (PTX-NPL5) with those of the other experimental drug nanocarriers functionalized by previously reported HCC cell-targeting aptamers and non-aptamer ligands, such as galactosamine and apotransferrin. A myriad of well-defined investigations such as cell cycle analysis, TUNEL (terminal deoxynucleotidyltransferase-mediated deoxyuridine triphosphate nick end labeling) assay, and studies related to apoptosis, histopathology, and immunoblotting substantiated that PTX-NPL5 had the highest potency among the different ligand-attached experimental formulations in inducing selective apoptosis in neoplastic hepatocytes via a mitochondrial-dependent apoptotic pathway. PTX-NPL5 did not produce any notable toxic effects in healthy hepatocytes, thus unveiling a new and a safer option in targeted therapy for HCC. Molecular modeling study identified two cell-surface biomarker proteins (tumor-associated glycoprotein 72 [TAG-72] and heat shock protein 70 [HSP70]) responsible for ligand-receptor interaction of L5 and preferential internalization of PTX-NPL5 via clathrin-mediated endocytosis in neoplastic hepatocytes. The potential of PTX-NPL5 has provided enough impetus for its rapid translation from the pre-clinical to clinical domain to establish itself as a targeted therapeutic to significantly prolong survival in HCC.

INTRODUCTION

Hepatocellular carcinoma (HCC), a widely diagnosed form of malignant cancer, has become a leading cause of death among cancer patients throughout the world.[1,2] During the development of HCC, alteration of several biochemical pathways causes sequential conversion of normal hepatocytes into malignant hepatocytes through the acquisition of several neoplastic characteristics such as uncontrolled cellular proliferation, activation of mitogenic signaling and disruption of the cellular death signaling pathway, promotion of epithelial-mesenchymal transitions, metastasis, angiogenesis, and chemoresistance.[3] HCC is normally diagnosed at the advanced stages in which chemotherapy remains a sole available option. However, the reduced ability of currently available chemotherapeutics to penetrate into neoplastic hepatocytes and their severe toxicity in healthy tissue greatly compromise the therapeutic outcome, as reflected by a high incidence of mortality.[1,4,5] Therefore, site-specific delivery of chemotherapeutics to neoplastic hepatocytes is the golden option to control the progress of the disease more efficiently and to overcome the cytotoxic effects of the chemotherapeutics to normal cells.[4–6] Thus, ligand-based active targeting strategies for the preferential delivery of therapeutic payloads into neoplastic hepatocytes have been attempted by researchers around the globe to achieve radical improvement in the therapeutic outcome in HCC.[1,2,5–7] Among the myriad of ligands explored by researchers for the development of targeted therapy against HCC, aptamer-mediated targeting of neoplastic hepatocytes has gained significant momentum over the targeting with other HCC cell-targeting ligands, such as antibody, peptide, galactosamine, and transferrin, due to certain well-characterized features of aptamers such as low molecular weight, greater specificity and affinity to the target molecules, non-immunogenicity, higher tissue penetration capability, thermostability,

Received 30 November 2019; accepted 29 January 2020;
https://doi.org/10.1016/j.omtn.2020.01.034.

[6]Present address: Department of Pharmacy, College of Medicine and health Science, Bahirdar University, Bahirdar, Ethiopia

Correspondence: Biswajit Mukherjee, PhD, Pharmaceutics Research Laboratory, Department of Pharmaceutical Technology, Jadavpur University, 188, Raja, S.C. Mullick Road, Kolkata 700032, West Bengal, India.
E-mail: biswajit.mukherjee@jadavpuruniversity.in

and the ease of modification and manufacturing.[2,8,9] Aptamers are short chemically synthesized DNA/RNA oligonucleotides. The unique three-dimensional structures of aptamers result in extremely high affinity and specificity for the target molecules, thus rendering them a highly promising ligand for the development of precision medicine.[8,9] Despite their enormous potential, to date, none of the aptamer-functionalized therapeutics against HCC has proved to be of clinical worth. Furthermore, the potential of a phosphorothioate-modified DNA aptamer, TLS 9a (L5 as named in the present investigation), for the site-specific delivery of therapeutics into the neoplastic hepatocytes has not been investigated so far despite its considerably low dissociation constant (K_D = 7.38 nM) that favors its high affinity toward its target.[1,2,10] We therefore intended to explore the potential of L5 to target neoplastic hepatocytes by comparing its efficacy with the previously reported aptamer ligands (L1–L4) and non-aptamer ligands (galactosamine/apotransferrin). They were attached on the surface of nanoparticles made up of biodegradable and US Food and Drug Administration (FDA)-approved poly(lactic-*co*-glycolic) acid (PLGA) polymer and evaluated with the help of numbers of *in vitro* and *in vivo* studies. A molecular modeling approach was performed to identify the cell-surface protein(s) responsible for the ligand-receptor interaction of L5 resulting in internalization of L5-functionalized drug nanocarrier in neoplastic hepatocytes. Furthermore, the investigation provides a special emphasis on the toxicological aspect of drug nanocarriers to develop a potent neoplastic hepatocyte-specific therapeutic without producing any notable toxic insult in normal hepatocytes. Mitotic spindle-targeting agent (MTA) such as paclitaxel (PTX) was used here as a model drug.[11]

RESULTS

Physicochemical Characterization of Experimental Nanoparticles

The multiple emulsion solvent-evaporation technique was performed to prepare PTX-loaded polymeric nanoparticles, as plenty of evidence in the literature suggested suitability of this technique to prepare stable drug-loaded nanoformulations capable of releasing drug sustainably for a prolonged time period.[12,13] D-α-Tocopherol polyethylene glycol succinate (TPGS) was used to increase the solubility of PTX, which in turn resulted in higher loading and entrapment efficacy.[14] Among the different nanoparticles prepared, the optimized ligand-free nanoformulation had drug loading and entrapment efficiency of 5.98% ± 0.55% and 67.31% ± 4.04%, respectively (Table S1). The formulation was selected for further study and designated as PTX-NP. The mean diameter and zeta potential of PTX-NP were found to be 181.5 ± 12.25 nm and −10.7 ± 4.27, respectively.

Aptamers (L1–L5) were conjugated on the surface of the nanoparticles, and they were designated as PTX-NPL1, PTX-NPL2, PTX-NPL3, PTX-NPL4, and PTX-NPL5 in the present study. The mean hydrodynamic diameters of aptamer-functionalized nanoparticles varied between 211.9 and 236.1 nm (Table S1). The amounts of aptamers conjugated to the surface of the nanoparticles were determined by UV spectroscopy. We found that 0.25 ± 0.05 nM L5, 0.23 ± 0.04 nM L2, 0.21 ± 0.034 nM L1, 0.18 ± 0.06 nM L4, and 0.19 ± 0.04 nM L3 per mg of PLGA nanoparticles were conjugated at the surface of the nanoparticles.[15]

The mean hydrodynamic diameter of galactosamine-functionalized nanoparticles (designated here as PTX-NPG) was found to be 240.9 ± 17.09 nm. A Morgan-Elson assay[16] showed that 62.16 ± 1.37 nM galactosamine/mg of nanoparticles was conjugated. For apotransferrin-conjugated nanoparticles (PTX-NPT1), the mean hydrodynamic diameter and zeta potential of PTX-NPT1 were found to be 242.4 ± 19.67 nm and −13.0 ± 5.46 mV respectively. The amount of apotransferrin conjugated to the nanoparticle surface was found to be 44.12 ± 2.16 nM as determined by the Bradford assay.

No substantial differences in PTX loading and entrapment efficiency of PTX-NP and different ligand-functionalized nanoparticles were observed, indicating that ligands did not enhance the loading and entrapment efficiencies of the experimental nanoparticles.

In Vitro Study

Cytotoxicity Study in Cancer and Normal Liver Cells

For *in vitro* study, along with the different ligand-functionalized nanoparticles, PTX-NP, free-drug suspension (PF), and commercial non-targeting formulation of PTX (Pacliall, Panacea Biotec), designated as MF, were evaluated.

Determination of IC_{50} (50% inhibitory concentration) doses by a 3-(4,5-dimethylthiazol-2-yl)-2,5-dimethyltetrazolium bromide (MTT) assay revealed that the cytotoxic potential of all of the experimental aptamer-functionalized nanoparticles was superior to PTX-NPT1/PTX-NPG. Among the different aptamer-functionalized nanoparticles, IC_{50} doses of PTX-NPL5 in HepG2 cells and Huh-7 cells provided the lowest values, suggesting the highest potency of PTX-NPL5 (Table S2). The same study in normal hepatocytes (Chang liver and WRL-68) had drastically opposite findings. PTX-NP and different aptamer-functionalized nanoparticles showed only 7%–9% inhibition of cell growth, even at their highest concentration (1 μM). PTX-NPG and PTX-NPT1 showed significant toxicity in normal hepatocytes, probably due to the significant expression of asialoglycoprotein and transferrin receptors, responsible for internalization of PTX-NPG and PTX-NPT1 via clathrin-mediated endocytosis.[17–21] MF was found to be maximally toxic against the normal hepatocytes, and we calculated IC_{50} doses of MF for normal hepatocytes only, which could not be calculated for other experimental formulations, as a minimum 50% of inhibition of cell growth is a prerequisite for the calculation of IC_{50} dose (Table S2). Blank nanoparticles did not exhibit any notable cytotoxic potential in neoplastic and normal hepatocytes, and therefore they were not considered for further studies. Cytotoxic potential of PTX-NP and PTX-NPL3 showed no appreciable difference. We therefore excluded PTX-NPL3 from further study.

Cell Cycle Analysis

Results of cell cycle analysis revealed that different experimental formulations caused cell arrest at the G_2/M and S phases, leading to the activation of three principal checkpoints of cell cycle,

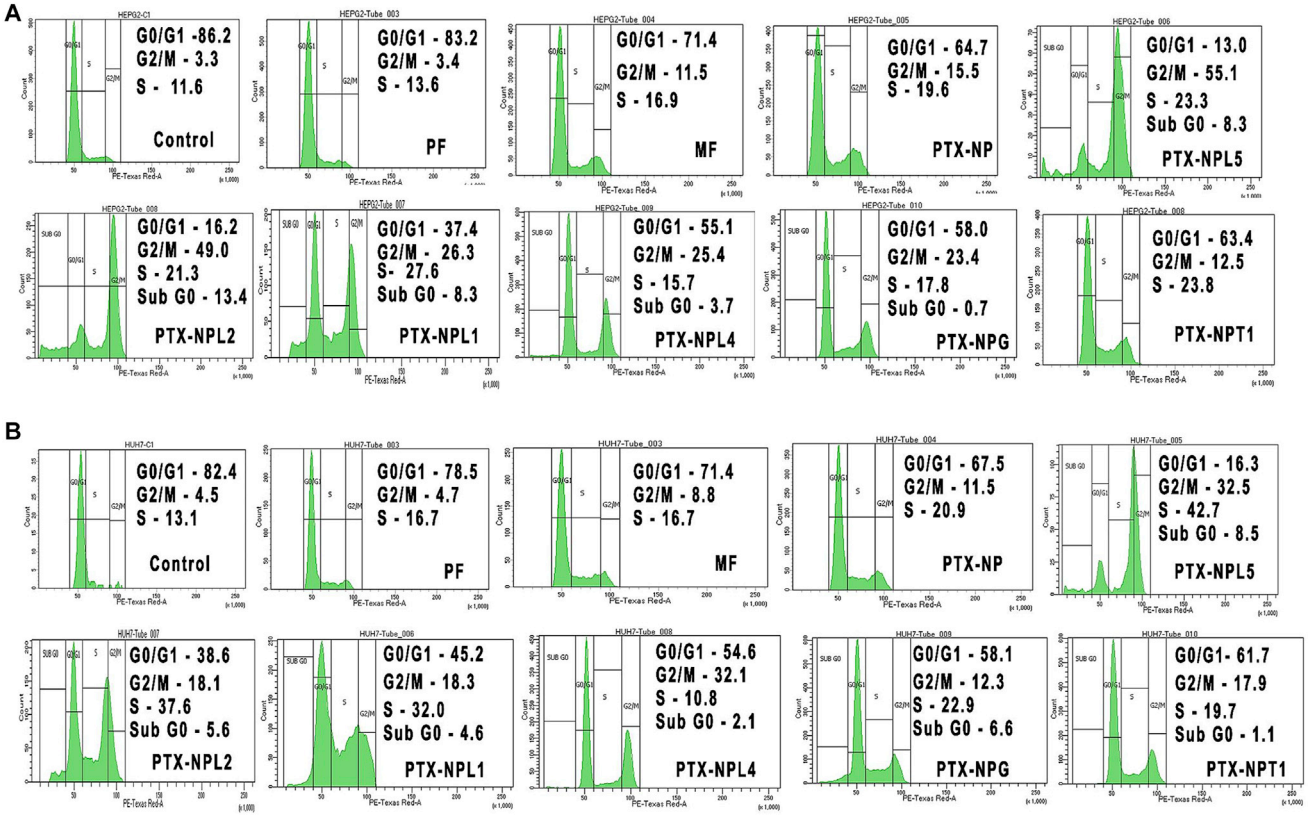

Figure 1. Cell Cycle Analysis in Neoplastic Hepatocytes

(A and B) Cell cycle data of (A) HepG2 cells and (B) Huh-7 cells upon treatment with different experimental formulations as mentioned within each block. Histograms represent percentages of cell arrest at different phases of the cell cycle. Cells without treatments were considered as controls.

namely, G_1/S, G_2/M, and spindle assembly checkpoints at metaphase/anaphase transitions (Figures 1A and 1B).[22,23] The maximum degree of cell arrest was observed in both types of cancer cells upon their treatment with PTX-NPL5. The comparative differentiation between the different investigated formulations to produce arrest of cells at the different phases of the cell cycle is provided in Figures 1A and 1B. G_2/M-phase arrest was probably due to the ability of PTX to stabilize microtubule assembly.[24] Fragmentation of DNA of neoplastic cells induced by different experimental formulations was probably the reason responsible for significant arrest at the S phase that led to the block of DNA replication and cellular proliferation of neoplastic hepatocytes. Flow cytometric data of cell cycle analysis clearly revealed that among the different ligand-functionalized nanoparticles, PTX-NPL1, PTX-NPL2, and PTX-NPL5 produced significantly high percentages of cell arrest at the S phase as compared to the G_2/M phase. Therefore, to confirm their more extensive DNA fragmentation potential as compared to other experimental nanoformulations and to compare their potential with MF, an Apo-5-bromo-2′-deoxyuridine (BrdU) DNA fragmentation *in situ* assay was performed. Findings of the investigation suggested that PTX-NPL5 was maximally effective in inducing DNA fragmentation (Figure S1) and transition of malignant hepatocytes toward apoptosis, thus reinforcing the findings of cell cycle analysis.[25,26]

Assessment of Cellular Apoptosis

Apoptosis is a highly regulated and well-characterized process with defined characteristic morphological features and biochemical changes. Thus, changes to determine apoptotic potential of different experimental formulations were investigated here.[27,28]

The downward shifting of mitochondrial membrane potential (MMP, $\Delta\psi m$) occurs very early in the apoptotic event, as opening of the mitochondrial permeability transition pore (MPTP) is the key to initiating the mitochondrial apoptotic pathway. This may be quantified by determining the reduction in values of the ratio of red to green fluorescence due to conversion of JC-1 aggregates (in viable cells with high MMP) to monomers (in apoptotic cells with lower MMP).[29,30] The decrement was maximal in neoplastic hepatocytes treated with PTX-NPL5, which signifies its highest apoptotic potential among the experimental formulations (Figures 2A and 2B).

Neoplastic cells, subjected to treatment with different experimental formulations, were dual stained with annexin V-fluorescein

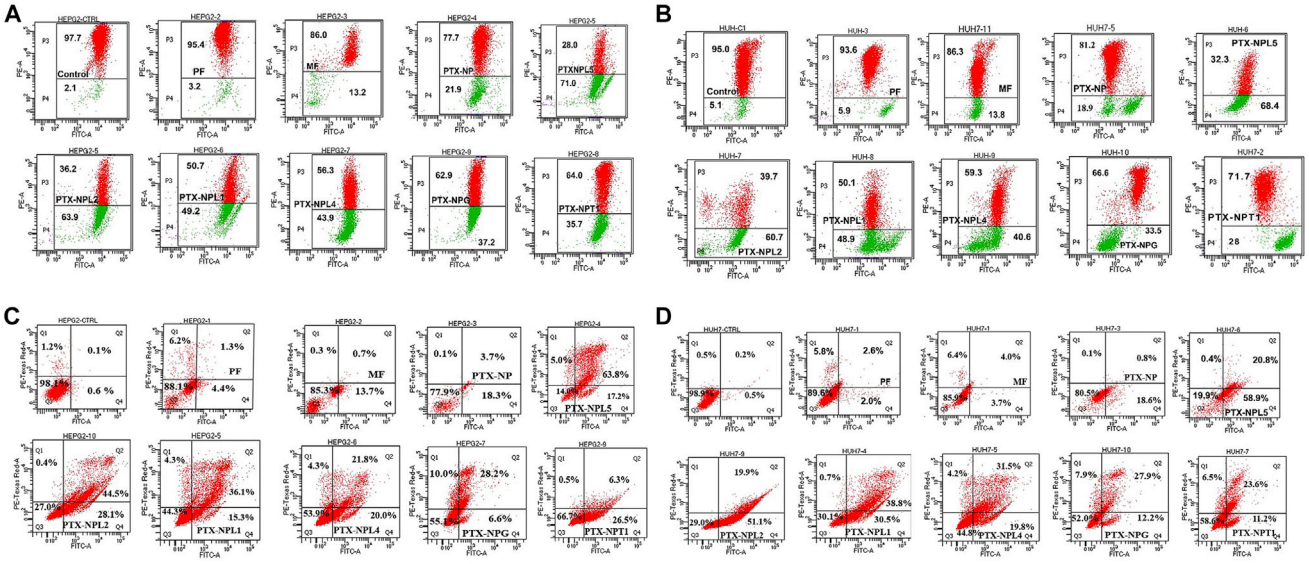

Figure 2. Determination of Changes in MMP in Neoplastic Hepatocytes and Quantifications of Apoptotic Cells upon Dual Staining with Annexin-V/FITC and PI

Quantitative determination of changes in mitochondrial membrane potential (MMP) by JC-1 staining and apoptotic/necrotic cells by an annexin V-FITC/PI dot plot assay upon treatment with different investigated formulations in HepG2 and Huh-7 cells, respectively, by flow cytometry. (A and B) Numbers denote the percentages of cell populations of malignant hepatocytes in P3 (live) and P4 (apoptotic) compartments upon treatment with different experimental formulations as mentioned within each block. Cells without treatment were considered as controls. (C and D) Percentages of cell populations of cancerous hepatocytes at different phases of apoptosis upon treatment with experimental formulations as mentioned within each block. (A and C) HepG2 cells. (B and D) Huh-7 cells. Q3, live; Q4, early apoptotic; Q2, late apoptotic; Q1, necrotic. Numbers denote the percentages of cell populations. The first block in the figures represents the control cells (cells without treatment).

isothiocyanate (FITC) and propidium iodide (PI), followed by quantification of apoptotic cells at different phases of apoptosis. Results of a dot plot assay supported earlier interpretations revealing maximum apoptotic potential of PTX-NPL5 among all of the investigated formulations (Figures 2C and 2D). The percentages of apoptotic cells upon treatment of HepG2 with PTX-NPL5 were found to be 63.8% (late apoptotic cells) and 17.2% (early apoptotic cells), whereas the percentages of apoptotic cells upon treatment of Huh-7 cells with the same were found to be 58.9% (early apoptotic cells) and 20.5% (late apoptotic cells).

Acridine orange/ethidium bromide (AO/EB) dual staining followed by visualization of apoptotic cells by confocal microscopy was performed to detect various types of apoptosis-induced morphological changes such as cell shrinkage, membrane blebbing, chromatin condensation, nuclear fragmentation, and formation of apoptotic bodies in cancerous hepatocytes upon treatment with different experimental formulations.[31–34] Upon staining, live cells appeared green, as they had taken up only AO. EB was taken up by cells that had lost their membrane integrity. Early apoptotic cells had a bright green nucleus and perinuclear chromatin condensation in the form of bright green patches or fragments. Late apoptotic cells were visible with orange to red nuclei with condensed or fragmented chromatin due to predominant uptake of EB. Necrotic cells stain red/orange, having resemblance in nuclear morphology of normal cells that have no chromatin condensation.[31–33] The distinct superiority of PTX-NPL5 over galactosamine/apotransferrin-functionalized nanoparticles (PTX-NPG/PTX-NPT1) in inducing apoptosis-mediated morphological changes in neoplastic hepatocytes was observed (Figures 3A and 3B). Furthermore, confocal imaging revealed the predominance of late apoptotic cells over early apoptotic cells. Comparative differentiations among the experimental formulations in inducing apoptosis-mediated morphological changes are given in Figures S2A and S2B.

Analysis of Toxicological Potential of Experimental Nanoparticles in Normal Hepatocytes

Severe toxicity of currently available chemotherapeutics in normal hepatocytes is one of the vital factors resulting in severe mortality of HCC patients.[1,5–7] Thus, one of the crucial aspects in the development of targeted therapy against HCC is to attack the neoplastic cells specifically without producing much harm to normal hepatocytes.

Morphological alterations of normal hepatocytes treated with different experimental formulations *in vitro* were analyzed by confocal microscopy upon dual staining with AO/EB. Results revealed that PTX-NPL5 showed no notable toxicity-related morphological changes in normal hepatocytes (Figures 4A and 4B). The other aptamer-functionalized nanoparticles showed an almost similar effect on the normal liver cells as shown by PTX-NPL5. The alterations of the morphology of normal hepatocytes

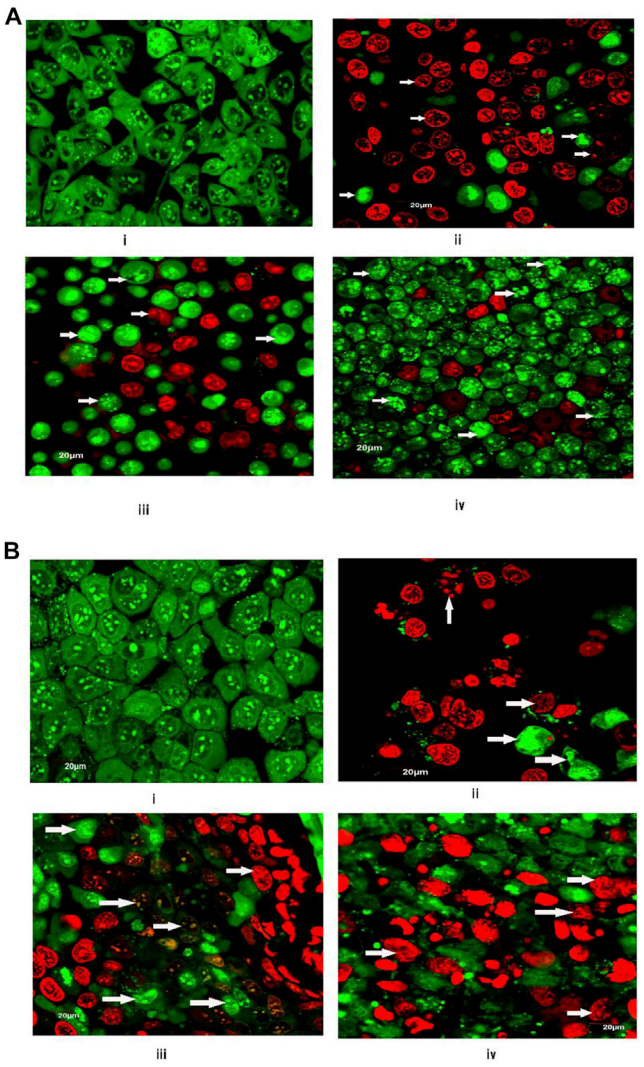

Figure 3. Apoptosis-Induced Morphological Alterations in Neoplastic Hepatocytes

(A and B) Confocal microscopic images depicting apoptosis-induced morphological alterations (indicated by arrows) upon treatment with different experimental formulations in (A) HepG2 cells and (B) Huh-7 cells. In (A) and (B), "i" represents the control (cells without treatment), and "ii–iv" represent cells treated with PTX-NPL5, PTX-NPG, and PTX-NPT1, respectively. Scale bars, 20 μm.

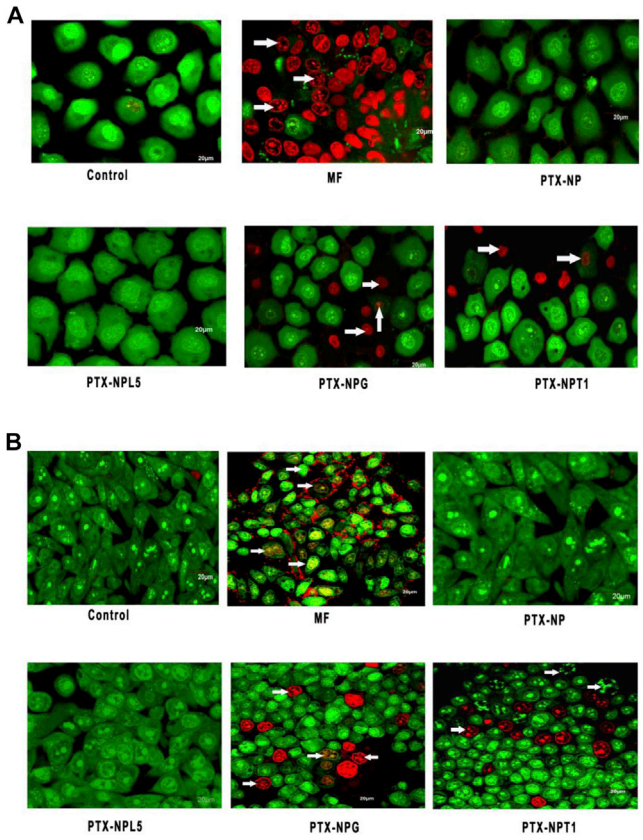

Figure 4. Confocal Images of Normal Hepatocytes upon Treatment with Different Experimental Formulations

Formulations are mentioned under each image. Scale bars, 20 μm. (A) Images of Chang liver cells. (B) Images of WRL-68 cells. Morphological changes such as nuclear fragmentation are indicated by arrows. Cells without treatment were considered as controls. Extensive changes were observed upon treatment with MF. No distinctive changes were observed between control cells and cells upon treatment with PTX-NPL5.

upon treatment with PTX-NPT1 and PTX-NPG were found to be distinctively greater as compared to aptamer-functionalized nanoparticles and PTX-NP (Figures 4A and 4B). Variable reactive oxygen species (ROS) levels were observed upon different experimental treatments (Figures S3A and S3B). The data are discussed in the Discussion.

In Vivo Study

For *in vivo* study, Sprague-Dawley (SD) male rats were placed in the following groups (six animals/group): group I, normal control rats; group II, carcinogen control rats; group III, carcinogen-treated rats receiving MF; group IV, carcinogen-treated rats receiving PTX-NPL5; group V, carcinogen-treated rats receiving PTX-NP; group VI, carcinogen-treated rats receiving PTX-NPL2; and group VII, carcinogen-treated rats receiving PF.

Macroscopic and Microscopic Hepatic Morphology of Experimental Rats

Hepatocarcinogenesis is a multistage complex process that arises from a background of chronic inflammation and fibrosis. Multiple genetic alterations occur in hepatocytes due to the chronic presence of carcinogen, leading to the clonal expansion of altered hepatocytes called hepatic-altered foci (HAF), which eventually transform to HCC. Through a series of biochemical and genetic alterations, HAF develop malignant cellular characteristics that transform into neoplasia. In the present investigations, different types of cancerous lesions[35–37] were considered to be HAF (Figure 5). Furthermore,

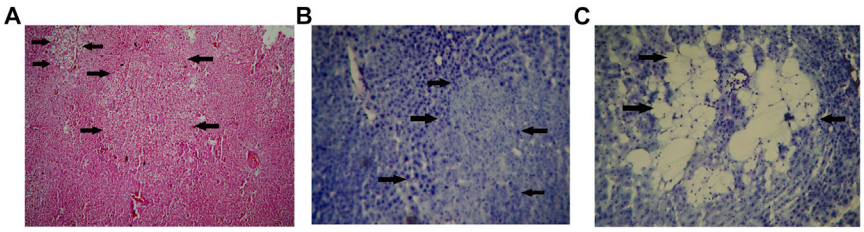

Figure 5. Microscopic Images of Liver of Rats Belonging to Carcinogen Control Groups

(A–C) Different changes in liver due to conversion of normal hepatocytes into neoplastic hepatocytes. Such alterations of highly differentiated HCC liver were considered as hepatic altered foci (HAF). (A–C) Ground-glass neoplastic lesions (A), basophilic neoplastic hepatic lesion (B), and spongiosis hepatis (C) (indicated by arrowheads) upon staining with hematoxylin and eosin (H&E) (A) and toluidine blue (B and C). Original magnification, ×100.

HAF were quantified per unit area (cm^2) of hepatic tissue. The occurrence of HAF was found to reduce in the liver of rats treated with different experimental formulations, and the reduction was found to be maximal (77%) in rats treated with PTX-NPL5 (group IV), without any tumor incidence (Table S3). The sizes of HAF in liver of rats treated with PTX-NPL5 reduced significantly as compared to their sizes in carcinogen control rats, as HAF in PTX-NPL5-treated neoplastic rats were found mostly to be <1 mm in size. The body weights of animals upon treatment with PTX-NPL5 were found to improve as compared to carcinogen control rats (Table S4). Histopathological examination of the liver of carcinogen control rats showed various types of HAF such as the appearance of ground glass cells, basophilic neoplastic lesions, and spongiosis hepatis, which are recognized as hallmark features revealing the sequential conversion of normal hepatocytes into malignant hepatocytes and the development of tumor in liver (Figure 5). The hepatic tissues of carcinogen-treated rats upon administration of different experimental treatments revealed the appearance of various apoptotic artifacts, and variable improvements of hepatocellular architecture were observed depending on the efficacy of the investigated formulations. All varieties of nanoparticles were found to be superior to MF and PF, possibly due to their ability to release PTX in a sustainable manner and deliver drug preferentially more to the target site. However, the curative potentials of PTX-NPL2 and PTX-NPL5 were distinctively superior to PTX-NP, possibly due to the affinity of L2 and L5 toward the cell surface biomarker proteins of neoplastic hepatocytes, leading to far superior internalization of PTX-NPL2 and PTX-NPL5 compared to PTX-NP. Furthermore, the comparison between therapeutic potentials of PTX-NPL2 and PTX-NPL5 on the basis of histopathological examination revealed that the efficacy of PTX-NPL5 was better than that of PTX-NPL2. This may be attributed to the superior interactions of L5 toward the surface biomarker proteins as compared to L2, resulting in superior internalization of PTX-NPL5 in comparison to PTX-NPL2. We have provided images of histopathological examination depicting extensive apoptosis in malignant hepatocytes and sequential as well as rapid improvement of hepatic architecture upon treatment with PTX-NPL5 during a period of 2 weeks (Figure 6A).

Analysis of Apoptotic Signaling Proteins

The mitochondrial apoptotic pathway is predominantly regulated by members of the Bcl-2 family, caspases, and the two key members of mitogen-activated protein kinases (MAPKs) such as c-Jun NH_2 terminal kinase (JNK) and p38. Immunoblotting analysis revealed the elevated levels of expression of Bak, phosphorylated forms of JNK and p38, caspase-3, and caspase-9, and downregulated expressions of Bcl-2 and Mcl-1 in the liver homogenates of carcinogen-treated rats treated with different experimental formulations as compared to carcinogen control rats (Figure 6B). Histograms representing the values of the ratio of expressions of Bak/Bcl-2, Bak/Mcl-1, phosphorylated JNK/total JNK, and phosphorylated p38/total p38 indicated that the values were maximal in livers of carcinogen-treated rats treated with PTX-NPL5, probably due its maximum internalization in neoplastic hepatocytes via receptor-mediated endocytosis.

In Vivo Toxicity Study

Complementary to *in vitro* study, *in vivo* assessment of the toxicological potential of experimental nanoparticles was carried out in accordance with established protocol,[38] and the results were in full agreement with the findings of *in vitro* investigations. No notable difference in the morphology of liver of normal Sprague-Dawley rats upon treatment with PTX-NPL5 was observed (Figure S4). Furthermore, examination of several biochemical parameters such as serum glutamate pyruvate transaminase (SGPT), serum glutamate oxaloacetate transaminase (SGOT), and alkaline phosphatase (ALK) of the normal Sprague-Dawley rats treated with different experimental formulations revealed that levels of toxicity were in the order of MF > PF > PTXNP~PTX-NPL5~PTX-NPL2, indicating extremely low toxicity of aptamer-functionalized nanoparticles in normal hepatocytes (Table S5). Furthermore, no significant changes in the body weight of normal rats treated with PTX-NPL5 were observed (Table S6). The extremely high toxicity of commercial formulation against normal rat liver highlighted the potential drawbacks of currently available chemotherapeutics for therapeutic management of HCC. Thus, powerful targeted therapy is badly needed to achieve a radical improvement in therapeutic outcome in HCC.

Hepatic Concentration of PTX in Normal and Carcinogen-Treated Rats upon Experimental Treatments

Upon treatment with different experimental formulations in normal rats, the maximum concentration of PTX (431.25 ± 7.73 ng/g) in the liver was obtained from commercial formulations, whereas PTX concentration was found to be significantly lower upon administration of aptamer-conjugated nanoparticles (PTXNPL5/ PTXNPL2) (Table S7). However, upon PF/MF treatment in carcinogen-treated rats, no predominant changes in concentrations of PTX were observed compared

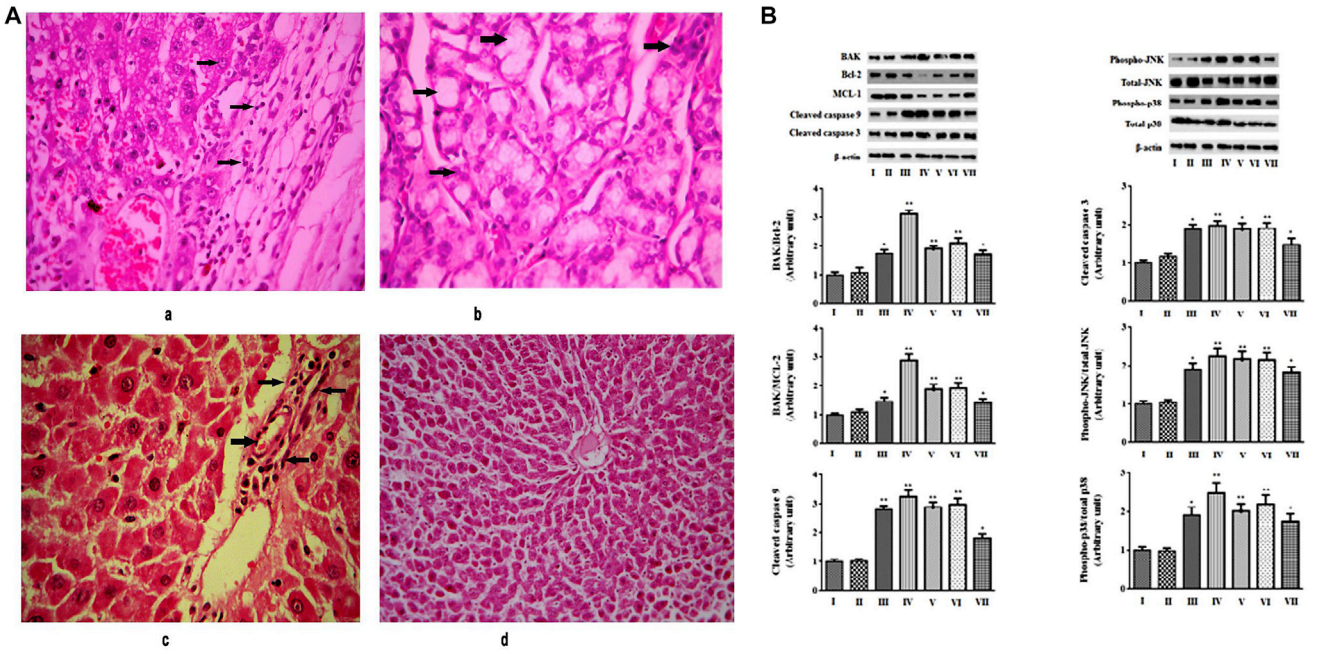

Figure 6. Histopathological Examinations of Liver of Carcinogen-Control Rats and Carcinogen-Treated Rats Treated with PTX-NPL5; and Immunoblotting of Some Apoptotic Signaling Proteins in Livers of Experimental Rats

(A) Histopathological images (H&E staining) of liver of carcinogen-treated rats treated with PTX-NPL5. (a) Induction of necrosis of normal hepatocytes and alignment of necrotic cells around the central vein in carcinogen control rats. Original magnification, ×400. (b) Ballooning of hepatocytes with an increase in perisinusoidal spaces and necrosis of normal hepatocytes in carcinogen control rats. Original magnification, ×400. (c) Initial improvement of hepatic architecture upon treatment with PTX-NPL5 and the presence of apoptotic cells around the central vein. Original magnification, ×400. (d) Predominantly improved restoration of liver architecture upon treatment with PTX-NPL5. Original magnification, ×100. (B) Western blots depicting expression of antiapoptotic and apoptotic signaling proteins in hepatic lysates of rats of different experimental groups. Numbers along the x axis denote different groups such as "I" for normal control rats, "II" for carcinogen control rats, and "III–VII" for carcinogen-treated rats treated with MF, PTXNP-L5, PTX-NP, PTX-NPL2, and PF, respectively. β-actin served as a loading control. Each value represents mean ± SD (n = 3). *$p < 0.05$, **$p < 0.01$ for differences between the normal control group and carcinogen-treated rats receiving various treatments. Histograms represent the ratio of values of apoptotic protein with respect to antiapoptotic proteins.

to the data for normal rats treated with MF/PF. A slight increase in concentrations of PTX from PF/MF that was observed at respective time points may be due to the alteration of liver morphology for the induction of carcinogenesis, which resulted in hindered clearance of the nanoparticles. The concentrations of PTX upon PTX-NP, PTX-NPL2, and PTX-NPL5 treatment were found to significantly increase as compared to their concentrations in normal rats. A drastically increased concentration of PTX from PTX-NPL2/PTX-NPL5 was observed, and it may be due to interactions of L5/L2 with the receptor proteins on the surface of neoplastic hepatocytes (Table S8).

Analysis of Aptamer-Receptor Protein Interactions by Molecular Docking

Molecular docking was performed to identify binding proteins of L5 on neoplastic hepatocytes and to analyze its probable interactions with these biomarker proteins to interpret affinity of L5 binding specifically to neoplastic hepatocytes. Furthermore, we compared the ligand-receptor interactions of L2 and L5 in order to find the reason behind the superior therapeutic potential of PTX-NPL5 compared to PTX-NPL2, even at the molecular level. Despite extensive efforts, the target proteins of L2 were hard to find in the literature. We conducted blind docking to identify the target proteins responsible for ligand-receptor interactions of L2 and L5. Based on docking scores, the number of amino acids responsible for binding interactions, and the calculation of binding energy to select the most stable conformations, we identified that heat shock protein 70 (HSP70) and tumor-associated glycoprotein 72 (TAG-72) were the most probable surface biomarker proteins responsible for ligand-protein interactions of L2 and L5, leading to preferential internalization of PTX-NPL5 and PTX-NPL2 in neoplastic hepatocytes (Figures 7A–7D). Furthermore, a computational modeling and ligand-receptor interaction study revealed superior interactions of L5 with these biomarker proteins as compared to L2. The reason underpinning this observation may be attributed to the participation of amino acids of receptor proteins to a greater extent for interacting with L5 than that with L2 (Table S9). This might result in better internalization and therapeutic potential of PTX-NPL5 than those of PTX-NPL2.

DISCUSSION

The long latent period, multidrug resistance, inadequate uptake of chemotherapeutics by malignant hepatocytes, severe toxicity of chemotherapeutics in normal and healthy cells, and growing incidence of

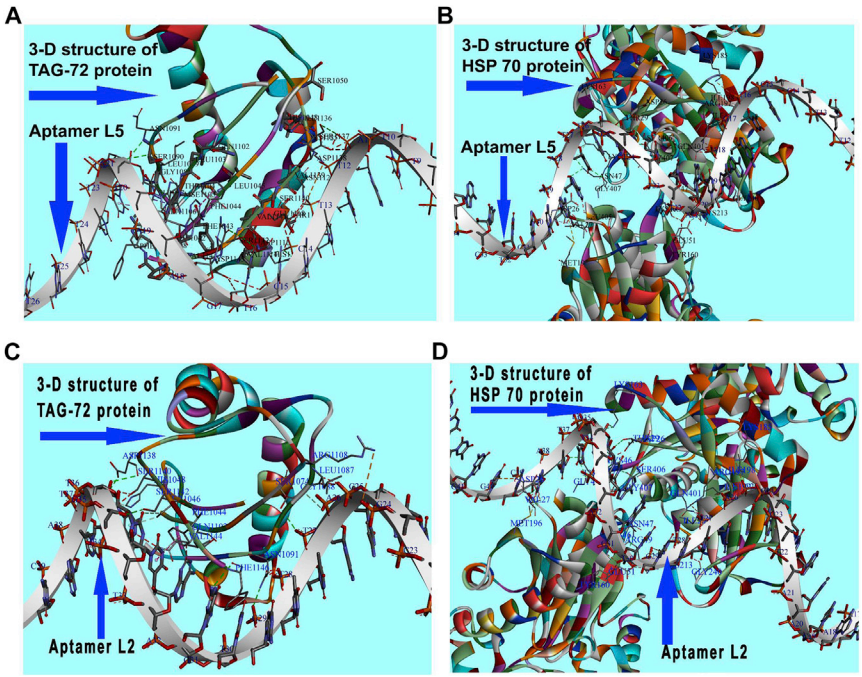

Figure 7. Images of Interactions of L5 and L2 with Surface Biomarker Proteins of Neoplastic Hepatocytes HSP70 and TAG-72

(A and B) Ligand-receptor interactions of L5 with TAG-72 (A) and HSP70 (B). (C and D) Ligand-receptor interactions of L2 with TAG-72 (C) and HSP70 (D).

HCC have led to a remarkably high mortality of HCC patients globally.[1,2,4–7] Despite several endeavors by researchers, none has succeeded in developing a site-specific delivery strategy for the preferential delivery of therapeutic payloads to neoplastic hepatocytes. A handful of those that had breakthroughs initially failed ultimately to yield effective results in clinical practice. There are certain ligand-related potential drawbacks such as incorrect choice of ligand, poor *in vivo* stability, high immunogenicity, and poor permeability of ligand that result in a feeble outcome.[1–5] Thus, to deliver a drug nanocarrier preferentially to neoplastic hepatocytes for powerful induction of neoplastic cell-specific apoptosis along with a remarkable reduction in toxicity of chemotherapeutics in normal healthy cells was the fundamental focus of the present investigation. Several reports revealing the potential of different aptamers for site-specific delivery of therapeutic payloads to neoplastic hepatocytes for achieving much better therapeutic outcome in HCC are available in the literature.[1,2] However, none of these studies has compared the potential of their investigated aptamers with the other already established malignant hepatocyte-targeting ligands. This study is the first of its kind that has shown a comparative efficacy between L5 and the other already reported malignant hepatocyte-targeting aptamers and the non-oligonucleotide ligands such as galactosamine and apotransferrin.

From an array of aptamers reported in the literature as HCC-targeting ligands,[10] we have chosen to investigate the aptamers L1–L5. L2 (TLS11a), one of the most popular aptamers to study owing to its low K_D value, was tried for aptamer-based targeted therapy against HCC.[1,2,10] Guanosine (G)-rich AS-1411 aptamer (L4), has been explored for its high binding ability to nucleolin overexpressed on malignant hepatocytes.[39] APS 613-1 (L1) was selected to target glypican 3 (GPC3), which is overexpressed especially on neoplastic hepatocytes and is considered as a potential biomarker for early diagnosis of HCC[40]. L3 was considered as a control aptamer. The parent structures of all of the aptamers were modified by the addition of the phosphorothioate backbone and amino group ($-NH_2$) at the 3′ end. Overexpressed asialoglycoprotein and transferrin receptors on HCC cells have been targeted with the ligands such as galactosamine and apotransferrin, respectively.[17,18] Based on *in vitro* investigations such as cytotoxicity, cell cycle analysis, and apoptotic potential in HCC cells and nontoxicity or less toxicity in normal cells, we selected L5 in the present study for further investigation to compare its efficacy in targeting neoplastic hepatocytes compared to the other non-aptamer HCC cell-targeting ligands such as apotransferrin and galactosamine.

Physical characterizations of experimental nanoparticles revealed that particles of all of the nanoformulations were in the nanometric range with a narrow polydispersity index (PDI), indicating homogeneous distribution of the experimental nanoparticles.[41]

Potency of L5 aptamer-functionalized nanoparticles proved to be significantly higher in comparison to galactosamine and apotransferrin functionalized nanoparticles, as evidenced by the IC_{50} doses of the different experimental formulations. Data on PTX-NPL3 and PTX-NP had nearly similar findings. Hence, we continued with PTX-NP instead of PTX-NPL3.

Cell arrest by chemotherapeutics at different phases of the cell cycle is reflected in the activation/inhibition of many signaling proteins, DNA repair, transcriptional regulation, and apoptosis. The inability of the signaling network to regulate the changes caused by chemotherapeutics in the malignant cells may lead the cells to apoptosis.[42] Thus, cell cycle analysis provides the first distinctive clue regarding initiation of the apoptotic pathway.[43] The findings on the cell cycle provided a clear-cut indication of extensive DNA fragmentation in neoplastic cells due to a distinctively higher percentage of cells at the S phase as compared to the other phases of the cell cycle, especially upon treatment with aptamer-functionalized nanoparticles. An Apo-BrdU *in situ* DNA fragmentation assay was performed to clarify the above-mentioned fact due to the ability of bromolated deoxyuridine triphosphate (Br-dUTP) to incorporate preferentially into DNA

strand breaks. The ability of fluorescein-labeled anti-BrdU antibody to specifically bind with Br-dUTP generates a fluorescent signal that can be measured by flow cytometry to assess quantitative differentiation in the DNA fragmentation potential.[25,26]

Much evidence suggests the primary role of the mitochondrial intrinsic apoptotic pathway in chemotherapy-induced apoptosis. ROS above the cellular tolerability threshold trigger the mitochondrial apoptotic pathway by disrupting the Ca^{2+} homeostasis between mitochondria and endoplasmic reticulum (ER) primarily due to their close proximity as well as oxidation of cardiolipin (one of the key lipids of mitochondrial membrane), resulting in massive influx of Ca^{2+} through the Ca^{2+} uniporter.[24,25] The rise of Ca^{2+} overload to a critical threshold results in the activation and opening of MPTP, as well as an increase in mitochondrial outer membrane permeability (MOMP).[26,27,44] The net outcome of these events is osmotic swelling and rupture of mitochondria, disruption of essential biochemical events, mitochondrial hyperpolarization and collapse of MMP, translocation of proapoptotic proteins into mitochondria, and release of mitochondrial transmembrane proteins, especially cytochrome *c* (cyt-c), followed by activation of the downstream caspase cascade that results in induction of apoptosis via mitochondrial-dependent pathway. Furthermore, oxidation of cardiolipin disrupts the attachment of cyt-c with the inner mitochondrial membrane (IMM) and increases the probability of its release into the cytosol to activate the apoptotic events.[26,27] Under normal physiological conditions, green monomer of JC-1 upon its entry into the cytosol of malignant cells undergoes aggression into mitochondria to form numerous red J aggregates.[29,30,45] The decrement in the values of the ratio of red to green fluorescence due to the conversion of JC-1 aggregates to JC-1 monomers indicates a loss of MMP and significant mitochondrial damage, and thus quantitative determination of decreased values directly correlates with the apoptotic potential of chemotherapeutics.

Significant advancements in the development of targeted nanomedicine have resulted in preferential delivery of therapeutic payloads into the subcellular compartments, namely, mitochondria, nucleus, lysosomes, and ER of neoplastic cells, due to their intimate correlation with cell growth, differentiation, and proliferation of targeted malignant cells/tissues for achieving much therapeutic outcome.[46] However, mitochondria of malignant hepatocytes are the selective organelles of attack in HCC due to the vulnerability of mitochondrial DNA (mtDNA) to ROS and an immaculate role of mutated mtDNA in the development of HCC.[47–52] Much evidence in the literature suggests that a dual effect of PTX on microtubules and mitochondria (via ROS-mediated oxidative damage) generates an adequate signal for apoptosis.[11,44] Furthermore, flow cytometric measurement of ROS levels in malignant hepatocytes upon treatment with experimental formulations by using 2′,7′-dichlorodihydrofluorescein diacetate (DCFDA) revealed that the maximum ROS level was achieved in malignant hepatocytes upon treatment with PTX-NPL5, probably due to the maximum internalization of PTX-NPL5 in neoplastic cells (Figures S5A and S5B), as PTX is known to enhance NADPH oxidase (NOX) to increase the ROS level beyond the cellular tolerability threshold of neoplastic hepatocytes.[48]

The translocation of phosphatidylserine (PTS) into the outer membrane because of loss of lipid asymmetry occurs early in the apoptosis process, even before the classical appearance of DNA fragmentation. Annexin V can bind with the PTS-expressing cells which helps in the detection of apoptotic cells. The attached fluorochrome, fluorescein isothiocyanate (FITC) in turn helps to quantify the population of cells at various phases, such as apoptosis/necrosis by flow cytometer[31,32,53]

Differential uptake of fluorescent dyes such as AO and EB by live and apoptotic cells is recognized as a state-of-the-art technique to analyze apoptosis-mediated morphological changes. The stems from its simplicity, rapidity (devoid of a cell fixation step), and accuracy and its ability for simultaneous determination of the apoptotic index and cell membrane integrity.[31–33,49,50] Therefore, dual staining with AO and EB were performed to analyze the morphological changes in neoplastic hepatocytes upon treatment with different experimental formulations.

In vitro examinations of toxicity in normal hepatocytes showed that PTX-NPG and PTX-NPT1 exhibited significantly higher toxicity as compared with aptamer-functionalized nanoparticles. The reason could be the higher expressions of asialoglycoprotein and transferrin receptors in normal hepatocytes as compared to receptors responsible of internalization of aptamer-functionalized nanoparticles. Thus, the choice of ligand is also very important for successful development of targeted therapy. The target protein should be minimally expressed in normal hepatocytes to prevent the significant penetration and toxicity of chemotherapeutics in normal hepatocytes.

Data from *in vitro* investigations showed distinctively superior performance of L5 over the other investigated aptamers in inducing preferential apoptosis in neoplastic hepatocytes. The reason could be due to its extremely low K_D value. Interestingly, superior performance of L5 over L2 was probably due to its much shorter chain length as compared to L2. Thus, chain length and K_D value may be equally important determining factors when developing aptamer-functionalized therapeutics. Among all of the aptamer-functionalized therapeutics except PTX-NPL3, the potency of PTX-NPL4 was found to be minimal, probably due to lesser affinity of L4 for neoplastic hepatocytes as compared to other tested aptamers (L1, L2, and L5). The control aptamer (L3) did not potentiate the internalization of drug nanocarrier within the neoplastic hepatocytes, as no significant differences were observed between the potency of PTX-NP and PTX-NPL3. Furthermore, the target receptor (nucleolin) of L4 is overexpressed in the tumors of other tissues as well, such as prostrate, brain, and breast, thus making L4 not an absolutely selective ligand for HCC.[51,52]

Despite that the amounts of galactosamine/apotransferrin conjugated to nanoparticles were higher compared to aptamer conjugation to the nanoparticles, the performance of aptamer-functionalized

nanoparticles was predominantly better compared to PTX-NPG and PTX-NPT1. The mean hydrodynamic diameter of galactosamine-conjugated nanoparticles (PTX-NPG)/apotransferrin-conjugated nanoparticles (PTX-NPT1) was found to be nearly 250 nm. As compared to the aptamer-conjugated nanoformulations, the hydrodynamic diameters of PTX-NPG/PTX-NPT1 were found to be greater, which may be because of the larger size of the respective ligands (apotransferrin [molecular mass, 76–81 kDa]/galactosamine [molecular weight, 179.171 g/mol]) conjugated on the nanoparticles, compared to aptamers that were much smaller in size. In fact, in our *in vitro* investigations, such as cell cycle analysis, TUNEL (terminal deoxynucleotidyltransferase-mediated deoxyuridine triphosphate nick end labeling) assay, and studies related to apoptosis, we found that the therapeutic potential of those two nanoparticles (PTX-NPG/PTX-NPT1) was predominantly lower than for the other experimental formulations, possibly because of the larger size and comparatively lower affinity of the ligands toward neoplastic hepatocytes. Hence, we discarded these two formulations for further *in vivo* investigations considering their lower potential toward neoplastic cells. Again, there were no significant differences in the amount of conjugation of different aptamers to the nanoparticle surface. However, the superiority of PTX-NPL5 over the other aptamer-functionalized nanoparticles was probably due to its high affinity and efficient binding with the target receptors, causing better internalization of PTX-NPL5 to provide better therapeutic action.

Mutated DNA along with histological fibrosis due to chronic inflammations is the backbone for HCC development.[35–37] We investigated *in vivo* the potential of the experimental formulations in the chemically induced hepatocarcinogenesis model in rodents. Carcinogen-induced hepatocarcinogenesis depicts all of the cellular, biochemical, and molecular alterations for transformation of normal hepatocytes into malignant hepatocytes, resembling the development of hepatocarcinogenesis in humans. Therefore, an investigation of the efficacy of aptamer-functionalized drug nanocarriers using the above model may accelerate its rapid translation from a pre-clinical trial to a clinical trial to develop a powerful neoplastic hepatocyte-specific therapeutic weapon against HCC in the near future. Based on the findings of our *in vitro* investigations and in consideration of ethical guidelines, we designed fewer treatment groups *in vivo* as compared to *in vitro*. The treatment groups that seemed to be extremely critical to explore *in vivo* HCC-targeting potential were the only ones taken. Since L5 showed the best targeting potential to neoplastic hepatocytes among the investigated formulations, PTX-NPL5 was considered for this study. L2 was also considered, as this is the most widely used aptamer and is considered to have the best HCC-targeting potential.

Execution of cell death via the mitochondrial apoptotic pathway requires overexpression of proapoptotic signaling proteins of the Bcl-2 family and activation of two key members of the MAPK family, namely JNK and p38 by phosphorylation, followed by activation of the caspase cascade.[27,28,44] Generation of ROS beyond the cellular tolerability threshold results in a dramatic increase in expressions and transcriptional/posttranscriptional activities of proapoptotic members of the Bcl-2 family.[27,28] The mitochondrial-resident protein Bak upon activation undergoes conformational changes leading to their conversion from inactive monomers to active high-molecular-weight oligomers. Activated Bak accelerates MOMP by forming a permeable channel, resulting in the release of apoptogenic factors such as cyt-c into cytosol, and it activates apoptotic protease activating factor 1 (Apaf-1) followed by the conversion of procaspase-9 to caspase-9. The activated Apaf-1/cyt-c/caspase-9 forms a cytosolic complex, the apoptosome, which activates downstream executioner caspases, namely, caspase-3, -6, and -7, resulting in complete execution of the intrinsic apoptotic pathway. Among the different executioner caspases, the role of caspase-3 is of prime importance, as it cleaves different intracellular substrates, resulting in biochemical destruction of cells and phenotypic changes associated with apoptotic events. The ability of PTX to stimulate the activity and expressions of proapoptotic proteins, caspase-3, phosphorylated JNK, and p38 favors it to interact dually with mitochondria and microtubules. The expressions of two important members of stress-activated mitogen kinase (MAPK) such as JNK and p38 were analyzed in the liver homogenates of rats belonging to different experimental groups, due to their prominent role in mitochondrial apoptotic pathway.[27,28,44] Excessive ROS generation beyond the cellular tolerability threshold activates the redox sensor apoptosis signal-regulating kinase-1 (ASK1), which is responsible for the conversion of unphosphorylated inactive forms of JNK and p38 into activated phosphorylated forms.[54] Once activated, JNK translocates into mitochondria, resulting in inactivation of antiapoptotic proteins and activation of proapoptotic proteins, thus setting up a platform for apoptosis of malignant hepatocytes via a mitochondrial-dependent pathway. Despite its central role in mitochondria to stimulate an intrinsic apoptotic pathway, its role in the ER on Bcl-2 family proteins is also crucial to promote the mitochondrial apoptotic pathway.[27,28] Furthermore, activated JNK stimulates Bim and promotes its release from the dynein motor complex. Activated Bim translocates into mitochondria and promotes Bax-mediated apoptosis. Thus, Bim is recognized as a molecular bridge, illustrating simultaneous action of PTX on microtubules and mitochondria.[27,28,44] Findings in the literature suggest that p38α, especially the most prevalent form of p38, acts as an essential inhibitor of cellular proliferation. Upon phosphorylation, it prevents the progression of cells through G_1/S and G_2/M checkpoints by several mechanisms, such as downregulation of cyclins, upregulation of cyclin-dependent kinase inhibitors, and modulation of p53.Therefore, we analyzed the expression and activity of antiapoptotic and proapoptotic members of the Bcl-2 family, caspases, and phosphorylated forms of JNK and p38 to assess the therapeutic potential of experimental formulations. Among the investigated formulations, data for PTX-NPL5 suggest that it had the maximum potential to increase the expression of various apoptotic proteins and to decrease the level of expression of antiapoptotic proteins studied herein.[55]

The findings of *in vitro* and *in vivo* studies suggest that PTX-NPL5 had the most therapeutic potential among the investigated formulations. Furthermore, we found that PTX-NPL5 was extremely less

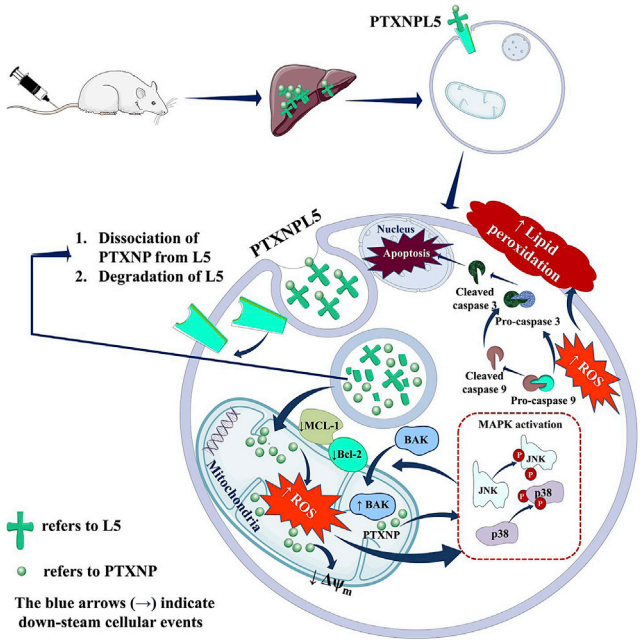

Figure 8. Schematic Representation of Internalization of PTX-NPL5 via Clathrin-Mediated Endocytosis upon the Interaction of L5 with TAG-72/HSP-70 as a Probable Mechanism of Action of PTX-NPL5

toxic against normal hepatocytes. The significantly high amount of hepatic availability of PTX in carcinogen-treated rats from PTX-NPL5/PTX-NPL2 compared to the other tested formulations indicates the superiority of these formulations (PTX-NPL5/PTX-NPL2) to deliver PTX predominantly in neoplastic hepatocytes. Hence, we predict in the present study that L5/L2 should have receptor proteins that specifically express/overexpress on the neoplastic hepatocytes. Thus, this offers a significant hope of developing a powerful targeted therapy against neoplastic hepatocytes to overcome the drawbacks associated with currently available chemotherapeutics.

We observed superior performance of PTX-NPL5 over PTX-NPL2 and interpreted that the shorter chain length of L5 could be a determining factor. To confirm this idea further, a molecular modeling study was performed to analyze the interactions of L5 and L2 with receptor proteins at the surface of neoplastic hepatocytes. Expression of TAG-72, a macromolecular glycoprotein, is significantly elevated in HCC as compared to normal tissue. The increased expression of TAG-72 is responsible for invasion and metastasis of HCC.[56,57] Among the different HSPs, overexpression of HSP27 and HSP70 was reported in HCC. HSP70 is recognized as a superior biomarker of HCC, as overexpression of HSP27 was reported only in HCC, upon its infection by hepatitis B virus (HBV). Evidence in the literature suggested that increased expression of 14-3-3σ promotes HCC tumor formation by inducing expression of HSP70, which promotes cellular proliferation via a β-catenin/heat shock factor-1 (HSF-1)-dependent pathway. Thus, expression of HSP70 is tightly controlled by the upstream regulator HSF-1 and the downstream regulator 14-3-3σ. Furthermore, conversion of normal hepatocytes to malignant hepatocytes is a multi-stage process starting from the appearance of pre-neoplastic lesions and ending with the appearance of tumors through various neoplastic lesions. Differential expression of HSP70 at different stages of HCC development makes it one of the potent biomarkers of HCC.[58,59] Thus, the ability of L2 and L5 to effectively interact with TAG-72 and HSP70 (which are minimally expressed in normal hepatocytes, whereas they show significantly high expression in neoplastic hepatocytes) makes them remarkably efficient ligands to preferentially target neoplastic hepatocytes. However, different parameters of computational modeling revealed more effective interaction of L5 as compared to L2, lending support to our hypothesis, as stated earlier, that chain length of the aptamer is also a crucial aspect in developing aptamer-based targeted therapy. Finally, we proposed a possible mechanism of action of PTX-NPL5 as follows. The interaction of L5 with TAG-72/HSP70 resulted in preferential accumulation of PTX-NPL5 in neoplastic hepatocytes. During internalization, it might move to a progressively more acidic compartment, followed by its arrival into lysosome for permanent degradation of the aptamer to set free the drug nanocarrier (Figure 8). Prolonged and sustainable release of PTX may result in an ROS-mediated attack on microtubule network and mitochondria in a concomitant manner, resulting in prolonged apoptosis.

In summary, phosphorothioate modified TLS 9a (L5) has shown its superiority over the tested experimental HCC cell-targeting ligands explored previously for the development of targeted therapy against HCC. The interactions of L5 with the surface biomarker proteins exclusively expressed by neoplastic hepatocytes provide a significant hope of developing an effective precision medicine to radically improve the survival of HCC patients in the near future.

MATERIALS AND METHODS

Acid-terminated PLGA (ratio, 75:25; molecular weight, 4,000–15,000 Da), *N*-nitrosodiethylamine (also known as diethylnitrosamine [DENA]), 2-acetylaminofluorene (2-AAF), TPGS, and apotransferrin were procured from Sigma-Aldrich (St. Louis, MO, USA). Culture media such as Dulbecco's modified essential medium (DMEM), minimum essential medium (MEM), fetal bovine serum, and penicillin-streptomycin (5,000 U/L) were purchased from Thermo Fisher Scientific (Waltham, MA, USA). Galactosamine, FITC, *N*-hydroxysuccinimide (NHS), 1-(3-dimethylaminopropyl)-3-ethylcarbodiimide hydrochloride (EDC), and MTT were procured from Himedia Laboratories (Maharashtra, Mumbai, India). Polyvinyl alcohol (PVA) (molecular weight, 125,000 g/mol) was bought from SD Fine Chemical (Maharashtra, Mumbai, India). An Apo-BrdU *in situ* DNA fragmentation assay kit was purchased from BioVision Technologies (Milpitas, CA, USA). MitoProbe JC-1 assay kit and FITC annexin V/dead cell apoptosis kit were procured from Thermo Fisher Scientific (Waltham, MA, USA). All of the reagents/chemicals used in this study were either of analytical grade or of molecular biology grade and utilized as received without further modification or purification.

Fresenius Kabi Oncology (Kolkata, West Bengal, India) provided PTX with 99.95% purity as a gift sample, and suspension of PTX was mentioned as free-drug suspension (PF). Pacliall injection (100-mg vial) from Panacea Biotec (Chandigarh, India), a commercial non-targeting formulation of PTX, was procured, and in the present investigation it was designated as MF. Aptamers (L1–L5) with phosphorothiate backbone modification and 3′-NH_2 modification were procured from GCC Biotech (West Bengal, India). Sequences of the studied aptamers are as follows: 37-base sequence (5′-TAACGCTGACCTTAGCTG CATGGTTTACATGTTCCA-3′-NH_2), designated here as L1; 63-base sequence (5′-ACAGCATCCCCATGTGAACAATCGCATTGTG ATTGTTACGGTTTCCGCCTCATGGACGTGCTG-3′-NH_2), designated here as L2; 45-base sequence control aptamer (5′-CACCGGG AGGATAGTTCGGTGGCTGTTCAGGGTCTCCTCCCGGTG-3′-NH_2), designated here as L3; 26-base sequence (5′-GGTGGTGGT GGTTGTGGTGGTGGTGG-3′-NH_2), designated here as L4; 39-base sequence (5′-AGTCCATTTTATTCCTGAATATTTGTTAACC TCATGGAC-3′-NH_2), designated here as L5.

Preparation of Nanoparticles

Multiple-emulsion solvent evaporation techniques were used for the preparation of experimental nanoparticles by following the protocol described in the literature with some modifications.[12,13] In short, 50 mg of polymer and TPGS (0.03% w/v) were added into the solvent mixture containing DCM and acetone at a ratio of 3:1 (v/v) followed by the addition of 5 mg of drug (PTX) into the solvent mixture after 30 min. The organic solution was emulsified by the dropwise addition of aqueous solution of PVA (2.5% w/v) under continuous homogenization at 20,000 rpm by using a high-speed homogenizer (model 10 basic Ultra-Turrax, IKA, Staufen, Germany) for a period of 6–8 min. The primary emulsion so formed was added to 75 mL of aqueous solution of 1.5% (w/v) PVA, and thus a multiple emulsion was formed. The prepared multiple emulsion was kept over a magnetic stirrer to remove residual organic solvent. The milky-white emulsion was centrifuged at 3,000 rpm in a refrigerated centrifuge (Hermle Labortechnik, Wehingen, Germany) to remove the macroparticles, and supernatant obtained from the previous centrifugation was further centrifuged at 16,000 rpm to obtain the aqueous precipitate of nanoparticles, which was further washed with Milli-Q water (Millipore, Billerica, MA, USA) to remove the residual PVA solution. Porous and dried nanoparticles were formed upon lyophilization of the precipitate in a freeze dryer (Instrumentation India, Kolkata, India), and they were stored in a freezer at −20°C. Optimized ligand-free nanoparticles based on physicochemical characterizations were designated as PTX-NP.

Various Ligand-Conjugated Nanoparticles

Aptamers (L1–L5) were conjugated on the surface of PTX-NP by following the protocol as described in the literature. Briefly, 5 mg of PTX-NP was washed with phosphate-buffered saline (PBS) of pH 7.4 and suspended in 250 μL of PBS. EDC (300 mM equivalent) and NHS (200 mM equivalent) were added to the mixture and then gently stirred for 2 h. Aptamers were dissolved in DNase/RNase-free water, which was denatured and renatured for 10 min and kept on ice for 20 min. The aptamers were then added to the mixture of nanoparticles and the mixture was incubated under gentle stirring for 6 h. The product was then washed three times with a washing solution (pH 8) composed of Tris-HCl and magnesium chloride, followed by centrifugation at 16,000 rpm to collect the washed final product. The end product was lyophilized and stored at −20°C.[15,60]

Apotransferrin (T1) was attached to the surface nanoparticles by using 250 μL of EDC and NHS at a concentration of 1 mg/mL. Briefly, 5 mg of PTX-NP was added in 2.5 mL of PBS followed by addition of EDC and NHS and stirred for 2 h. 100 μL of apotransferrin solution (1 mg/mL) was added dropwise to the suspension of the nanoparticles and incubated for 4 h at room temperature. The unbound apotransferrin was removed by ultracentrifugation at 25,000 × *g* using an Avanti J-301 centrifuge (Beckman Coulter, CA, USA). The apotransferrin-conjugated nanoparticles (PTX-NPT1) were lyophilized and stored at −20°C for further study. The quantitative estimation of apotransferrin conjugated to nanoparticles was performed by using a Bradford assay with Coomassie blue G as described in the literature.[53,61] The amount of apotransferrin conjugated was expressed as nM/mg of nanoparticles.[21,53]

Galactosamine (G) was conjugated at the surface of the nanoparticles by using EDC and NHS. Briefly, galactosamine at a concentration of 1 mg/mL was added to the suspension of nanoparticle-containing EDC and NHS and incubated as described previously. The unconjugated galactosamine was separated by ultrafiltration, and the galactosamine-conjugated nanoparticles (PTX-NPG) were lyophilized and stored at −20°C for future use. The amount of galactosamine conjugated to the surface of the nanoparticles was expressed as nM/mg of nanoparticles.[16–20]

Physicochemical Characterizations of Experimental Nanoparticles

Size distribution, PDI, and zeta potential of the freeze-dried experimental nanoparticles were determined by Zetasizer Nano ZS (0.6–600 nm) using DTS software v4.0 (Malvern Instruments, Worcestershire, UK) upon suspending them in Milli-Q water.

Accurately weighed nanoparticles were added in a mixture of acetonitrile and water in a ratio of 60:40 (v/v). The mixture was vortexed to form uniform dispersion and kept in an incubator shaker (Somax incubator shaker; Shenzhen Pango Electronic Company, Henggang, China) for 4 h. The suspension of nanoformulations was centrifuged at 16,000 rpm at 4°C, and the supernatant thus obtained was analyzed by high-performance liquid chromatography (HPLC) using a C_{18} analytical column, operated at 30°C with a flow rate of 1 mL/min, with detection at 227 nm. The analysis was performed in triplicates. Percentages of drug-loading and entrapment efficiency were determined by the formula as described in the literature.[12,13]

In Vitro Study

Cancerous hepatocytes (HepG2 and Huh-7 cells) and normal hepatocytes (Chang liver cells and WRL-68 cells) procured from the

National Centre for Cell Sciences (NCCS, Pune, India) were used in the study. HepG2 and Huh-7 cells in DMEM with high glucose and Chang liver cells and WRL-68 cells in Eagle's minimum essential medium and supplemented with 10% (v/v) FBS were maintained. The cells were kept in a humidified CO_2 incubator (New Brunswick Scientific, Edison, NJ, USA) at 37°C.

Cytotoxicity Study

Cell suspensions (100 μL) of respective cell lines (3×10^4 cells/mL) were added to each well of 96-well tissue culture plates, and plates were kept in an incubator. On the next day, complete medium was replaced by incomplete medium and cells were treated with different experimental formulations at a concentration of 10 nm to 1 μM. The effect of different experimental formulations on the viability of cells was determined by MTT assay. IC_{50} doses of different experimental formulations were determined from the data of cell viability as described in the literature.[31,32]

Cell Cycle Analysis

To investigate the effects of different experimental formulations on cellular proliferation of neoplastic hepatocytes, cell cycle analysis was performed. Seeding of the cells at a concentration of 1×10^6 cells/well was done in a 12-well plate, which was kept in a CO_2 incubator overnight. Cell cycle phase distributions of PI-stained nuclear DNA of neoplastic hepatocytes were performed in a flow cytometer (Becton Dickinson FACS Fortessa 4 laser cytometer with the use of BD FACSDiva software) upon their treatment with different experimental formulations as mentioned in the literature.[32,53]

DNA Fragmentation Analysis

HepG2 and Huh-7 cells (1×10^6/mL) were allowed to grow and were treated with different treatments as described earlier. DNA fragmentation analysis was performed by an Apo-BrdU *in situ* DNA fragmentation assay kit (BioVision Technologies, Milpitas, CA, USA) as per the manufacturer's protocol, and fluorescent signals were measured by a flow cytometer.

Assessment of Cellular Apoptosis

Apoptosis-induced morphological changes in cancerous hepatocytes were determined by confocal microscopy (FluoView FV10i confocal laser microscope, Olympus, USA) upon treatment of the neoplastic hepatocytes with IC_{50} doses of the investigated formulations.

A MitoProbe JC-1 assay kit (Thermo Fisher Scientific, USA) was used to assess the changes in MMP ($\Delta\psi m$) as a result of apoptosis. Briefly, cells were allowed to grow in 12-well plates at a concentration of 1×10^6 cells/per well. The manufacturer's protocol was followed, and quantitative determination of changes in MMP was performed by measuring the associated fluorescence in a flow cytometer.

A FITC annexin V/dead cell apoptosis kit (Thermo Fisher Scientific, USA) was used to analyze the neoplastic cells at the different phases of apoptosis and necrotic zone upon treatment with the different experimental formulations. Quantitative determination was performed using a flow cytometer.

Determination of ROS

Neoplastic hepatocytes (HepG2 and Huh-7 cells) treated with experimental formulations were allowed to grow at 37°C in a CO_2 incubator for 24 h. Measurement of ROS was performed with a cellular ROS assay kit as per the manufacturer's instructions (Abcam, USA) and analyzed quantitatively by a flow cytometer.

Toxicity Study in Normal Hepatocytes

Toxicological potentials of experimental formulations toward normal hepatocytes were studied upon the analysis of cellular morphology of normal hepatocytes (Chang liver cells and WRL-68 cells) treated with different experimental formulations. Before confocal imaging, cells were dual stained with AO/EB.[31–33]

In Vivo Study

All animal experiments were approved by the Institutional Animal Ethics Committee (AEC), Jadavpur University and conducted following the guideline of the AEC. Animals were divided into different groups containing six rats in each group as follows: group I, normal control rats; group II, carcinogen control rats; group III, carcinogen-treated rats receiving MF; group IV, carcinogen-treated rats receiving PTX-NPL5; group V, carcinogen-treated rats receiving PTX-NP; group VI, carcinogen-treated rats receiving PTX-NPL2; and group VII, carcinogen-treated that receiving PF (Figure S5).

Hepatocarcinogenesis in rodents was developed by using DENA as an initiator and 2-AAF as a promoter. DENA was given at the beginning of the experiment intraperitoneally at a dose of 200 mg/kg body weight. 2-AAF treatment was started at the third week and continued up to 20 weeks. 2-AAF (0.5% w/w) was given by mixing it with small quantities of food in the morning followed by the basal diet.[62,63] Different treatments such as MF, PTX-NP, PTX-NPL2, and PTX-NPL5 (equivalent to PTX, 10 mg/kg body weight) were given via an intravenous (i.v.) bolus injection at the end of the 36th week, and the treatments were continued at an interval of 3–4 days for a period of 14 days. Cervical dislocation under ketamine-xylene anesthesia was performed to euthanize the animals after completion of the treatment schedule. Livers were removed from the rats belonging to different treatment groups used for *in vivo* study. The collected liver samples were sliced, snap-frozen in liquid nitrogen, and stored in an ultra-low freezer (U4 lo, New Brunswick Scientific, CT, USA) for further use.

Morphological Examination of Liver

Macroscopic examination of tissue samples collected from normal control rats, carcinogen-treated rats, and carcinogen-treated rats receiving different treatments was performed to examine for the presence of tumors and hyperplastic nodules, which were identified and demarcated from reddish-brown non-nodular surroundings due to their characteristic grayish-white, darkish-red color and bulging-out growth.

Furthermore, serial sectioning of livers (6 μm) was done and sections were further processed histochemically by toluidine blue and hematoxylin and eosin for investigating microscopic changes in tissue architectures, including pre-neoplastic and neoplastic lesions. Hepatic lesions were identified as HAF and classified as clear ER-rich foci (ground glass appearance), mixed cell foci, and ribosome-rich basophilic foci. The number and area of the lesions were determined by a Zeiss light microscope and analyzed by AxioVision software v4.7.1.[62,63]

Western Blotting

Frozen liver tissue samples (approximately 60 mg) collected from liver tissues of normal control rats (group I), carcinogen control rats (group II), and carcinogen-treated rats receiving various treatments as mentioned earlier were processed into different cellular fractions to isolate, namely, cytosolic, microsomal, and nuclear fractions. The expressions of bcl-2, bak, Mcl-1, cleaved caspase-9, cleaved caspase-3, total JNK, phosphorylated JNK (Tyr183/Tyr185), total p38, and phosphorylated p38 (Tyr180/Tyr182) were estimated.[64–67]

In Vivo Toxicity Assessment in Normal Hepatic Tissue

An *in vivo* cytotoxicity study was carried out in the rats in a 28-day time frame.[35] The blood samples were collected from the tail vein at day 0 and day 28 upon i.v. bolus injection of PF/MF, PTX-NP, and PTX-NPL2 under aseptic conditions.[60] Blood samples were collected and allowed to stand for 30 min without any anticoagulant. The serum was collected after spinning the blood samples at 2,500 rpm for 10 min. Different biochemical parameters of the liver, such as SGOT, SGPT, and ALT, were determined by using a commercially available assay kit for these biochemical parameters as per the manufacturer's instructions.

Determination of Hepatic PTX Concentration upon Experimental Treatments

The concentration of PTX in the liver homogenates of normal and carcinogen-treated Sprague-Dawley rats were measured at 1, 2, 4, 6, 8, 10, 24, and 48 h by liquid chromatography-tandem mass spectrometry (LC-MS/MS) upon i.v. administration of PF/MF, PTX-NP, PTX-NPL2, and PTX-NPL5 at a dose equivalent to PTX dose, i.e., 10 mg/kg body weight) following the protocol as described in the literature.[12,13]

Computational Modeling to Analyze Ligand-Protein Interaction

A molecular docking study was performed to analyze ligand-receptor interactions of L2 and L5 (Figure S6). For this purpose, we downloaded 118 hepatocyte proteins from a protein databank (http://www.rcsb.org/). We used Biovia Discovery Studio 4.1 Client (http://www.3dsbiovia.com/products/collaborative-science/biovia-discoverystudio/visualization-download.php) to prepare the proteins and oligonucleotides (as ligands) and enabled all rotatable bonds (backbone phi and psi). To avoid any possibility of bias, the ligands were then randomized using the Biovia Discovery Studio 4.1 Client "randomize only" parameter to generate random starting respective poses different from the experimental ligands. Moreover, for every complex, we have used the same stochastic search seed for both the small and large search spaces and all of the tested configurations. After preparing the benchmarking dataset, we profiled the performances of the HDOCK blind docking server (http://hdock.phys.hust.edu.cn) on the dataset. The initial step of the docking protocol was to provide inputs for the receptor and the ligand. The server accepts both the sequences and structures as input for the protein and the oligonucleotide. The quality of a predicted protein-nucleotide binding mode is measured by its docking score. Docking analysis was performed using Biovia Discovery Studio 4.1 Client (http://www.3dsbiovia.com/products/collaborative-science/biovia-discoverystudio/visualization-download.php) software.[68]

SUPPLEMENTAL INFORMATION

Supplemental Information can be found online at https://doi.org/10.1016/j.omtn.2020.01.034.

CONFLICTS OF INTEREST

The authors declare no competing interests.

ACKNOWLEDGMENTS

The authors are grateful to the University Grants Commission (UGC), New Delhi, India, for providing financial assistance under the scheme UPE-II (Natural Products and Drug Delivery), reference 1-10/2012(NS/PE). The authors are also thankful to the Director, CSIR-IICB, Kolkata, India and Prof. Kunal Roy, Department of Pharmaceutical Technology, Jadavpur University, Kolkata, India for availing some facilities for successful completion of research. The authors also acknowledge Ms. Banasri Das, Ms. Debolina Chakraborty, Mr. Tanmoy Doloi, Mr. T. Muruganandan, and Mr. Binayak Pal (staff, Central Instrumentation Facilities, CSIR-IICB, Kolkata) for their useful help during this study.

REFERENCES

1. Li, M., Zhang, W., Wang, B., Gao, Y., Song, Z., and Zheng, Q.C. (2016). Ligand-based targeted therapy: a novel strategy for hepatocellular carcinoma. Int. J. Nanomedicine *11*, 5645–5669.
2. Ladju, R.B., Pascut, D., Massi, M.N., Tiribelli, C., and Sukowati, C.H.C. (2017). Aptamer: a potential oligonucleotide nanomedicine in the diagnosis and treatment of hepatocellular carcinoma. Oncotarget *9*, 2951–2961.
3. Trachootham, D., Alexandre, J., and Huang, P. (2009). Targeting cancer cells by ROS-mediated mechanisms: a radical therapeutic approach? Nat. Rev. Drug Discov. *8*, 579–591.
4. Chen, S., Cao, Q., Wen, W., and Wang, H. (2019). Targeted therapy for hepatocellular carcinoma: challenges and opportunities. Cancer Lett. *460*, 1–9.
5. Mohamed, N.K., Hamad, M.A., Hafez, M.Z.E., Wooley, K.L., and Elsabahy, M. (2017). Nanomedicine in management of hepatocellular carcinoma: challenges and opportunities. Int. J. Cancer *140*, 1475–1484.
6. Galun, D., Srdic-Rajic, T., Bogdanovic, A., Loncar, Z., and Zuvela, M. (2017). Targeted therapy and personalized medicine in hepatocellular carcinoma: drug resistance, mechanisms, and treatment strategies. J. Hepatocell. Carcinoma *4*, 93–103.
7. Zhang, X., Ng, H.L.H., Lu, A., Lin, C., Zhou, L., Lin, G., Zhang, Y., Yang, Z., and Zhang, H. (2016). Drug delivery system targeting advanced hepatocellular carcinoma: current and future. Nanomedicine (Lond.) *12*, 853–869.
8. Sun, H., Zhu, X., Lu, P.Y., Rosato, R.R., Tan, W., and Zu, Y. (2014). Oligonucleotide aptamers: new tools for targeted cancer therapy. Mol. Ther. Nucleic Acids *3*, e182.
9. Zhu, G., and Chen, X. (2018). Aptamer-based targeted therapy. Adv. Drug Deliv. Rev. *134*, 65–78.

10. Shangguan, D., Meng, L., Cao, Z.C., Xiao, Z., Fang, X., Li, Y., Cardona, D., Witek, R.P., Liu, C., and Tan, W. (2008). Identification of liver cancer-specific aptamers using whole live cells. Anal. Chem. *80*, 721–728.

11. Rovini, A., Savry, A., Braguer, D., and Carré, M. (2011). Microtubule-targeted agents: when mitochondria become essential to chemotherapy. Biochim. Biophys. Acta *1807*, 679–688.

12. Bhattacharya, S., Mondal, L., Mukherjee, B., Dutta, L., Ehsan, I., Debnath, M.C., Gaonkar, R.H., Pal, M.M., and Majumdar, S. (2018). Apigenin loaded nanoparticle delayed development of hepatocellular carcinoma in rats. Nanomedicine (Lond.) *14*, 1905–1917.

13. Mandal, D., Shaw, T.K., Dey, G., Pal, M.M., Mukherjee, B., Bandyopadhyay, A.K., and Mandal, M. (2018). Preferential hepatic uptake of paclitaxel-loaded poly-(D-L-lactide-*co*-glycolide) nanoparticles—a possibility for hepatic drug targeting: pharmacokinetics and biodistribution. Int. J. Biol. Macromol. *112*, 818–830.

14. Duhem, N., Danhier, F., and Préat, V. (2014). Vitamin E-based nanomedicines for anti-cancer drug delivery. J. Control. Release *182*, 33–44.

15. Yu, C., Hu, Y., Duan, J., Yuan, W., Wang, C., Xu, H., and Yang, X.D. (2011). Novel aptamer-nanoparticle bioconjugates enhances delivery of anticancer drug to MUC1-positive cancer cells in vitro. PLoS ONE *6*, e24077.

16. David, A., Kopecková, P., Rubinstein, A., and Kopecek, J. (2001). Enhanced biorecognition and internalization of HPMA copolymers containing multiple or multivalent carbohydrate side-chains by human hepatocarcinoma cells. Bioconjug. Chem. *12*, 890–899.

17. Pranatharthiharan, S., Patel, M.D., Malshe, V.C., Pujari, V., Gorakshakar, A., Madkaikar, M., Ghosh, K., and Devarajan, P.V. (2017). Asialoglycoprotein receptor targeted delivery of doxorubicin nanoparticles for hepatocellular carcinoma. Drug Deliv. *24*, 20–29.

18. Liang, H.-F., Yang, T.-F., Huang, C.-T., Chen, M.-C., and Sung, M.-C. (2005). Preparation of nanoparticles composed of poly(γ-glutamic acid)-poly(lactide) block copolymers and evaluation of their uptake by HepG2 cells. J. Control. Release *105*, 213–225.

19. D'Souza, A.A., and Devarajan, P.V. (2015). Asialoglycoprotein receptor mediated hepatocyte targeting—strategies and applications. J. Control. Release *203*, 126–139.

20. Willoughby, J.L.S., Chan, A., Sehgal, A., Butler, J.S., Nair, J.K., Racie, T., Shulga-Morskaya, S., Nguyen, T., Qian, K., Yucius, K., et al. (2018). Evaluation of GalNAc-siRNA conjugate activity in pre-clinical animal models with reduced asialoglycoprotein receptor expression. Mol. Ther. *26*, 105–114.

21. Malarvizhi, G.L., Retnakumari, A.P., Nair, S., and Koyakutty, M. (2014). Transferrin targeted core-shell nanomedicine for combinatorial delivery of doxorubicin and sorafenib against hepatocellular carcinoma. Nanomedicine (Lond.) *10*, 1649–1659.

22. Borel, F., Lacroix, F.B., and Margolis, R.L. (2002). Prolonged arrest of mammalian cells at the G1/S boundary results in permanent S phase stasis. J. Cell Sci. *115*, 2829–2838.

23. Yi, X., Zhang, X., Jeong, H., Shin, Y.-M., Park, D.-H., You, S., and Kim, D.-K. (2014). Novel bispidinoneanalog induces S-phase cell cycle arrest and apoptosis in HeLa human cervical carcinoma cells. Oncol. Rep. *33*, 1526–1532.

24. Priyadarshini, K., and Keerthi Aparajitha, U. (2012). Paclitaxel against cancer: a short review. Med. Chem. *2*, 139–141.

25. Ji, K., Lin, K., Wang, Y., Du, L., Xu, C., He, N., Wang, J., Liu, Y., and Liu, Q. (2018). TAZ inhibition promotes IL-2-induced apoptosis of hepatocellular carcinoma cells by activating the JNK/F-actin/mitochondrial fission pathway. Cancer Cell Int. *18*, 117–132.

26. Yao, Y., Dou, C., Lu, Z., Zheng, X., and Liu, Q. (2015). MACC1 suppresses cell apoptosis in hepatocellular carcinoma by targeting the HGF/c-MET/AKT pathway. Cell. Physiol. Biochem. *35*, 983–996.

27. Redza-Dutordoir, M., and Averill-Bates, D.A. (2016). Activation of apoptosis signalling pathways by reactive oxygen species. Biochim. Biophys. Acta *1863*, 2977–2992.

28. Indran, I.R., Tufo, G., Pervaiz, S., and Brenner, C. (2011). Recent advances in apoptosis, mitochondria and drug resistance in cancer cells. Biochim. Biophys. Acta *1807*, 735–745.

29. Chakraborty, B., Dutta, D., Mukherjee, S., Das, S., Maiti, N.C., Das, P., and Chowdhury, C. (2015). Synthesis and biological evaluation of a novel betulinic acid derivative as an inducer of apoptosis in human colon carcinoma cells (HT-29). Eur. J. Med. Chem. *102*, 93–105.

30. Saneja, A., Kumar, R., Singh, A., Dhar Dubey, R., Mintoo, M.J., Singh, G., Mondhe, D.M., Panda, A.K., and Gupta, P.N. (2017). Development and evaluation of long-circulating nanoparticles loaded with betulinic acid for improved anti-tumor efficacy. Int. J. Pharm. *531*, 153–166.

31. Paul, A., Das, S., Das, J., Samadder, A., and Khuda-Bukhsh, A.R. (2013). Cytotoxicity and apoptotic signalling cascade induced by chelidonine-loaded PLGA nanoparticles in HepG2 cells in vitro and bioavailability of nano-chelidonine in mice in vivo. Toxicol. Lett. *222*, 10–22.

32. Nandi, D., Besra, S.E., Vedasiromoni, J.R., Giri, V.S., Rana, P., and Jaisankar, P. (2012). Anti-leukemic activity of *Wattakaka volubilis* leaf extract against human myeloid leukemia cell lines. J. Ethnopharmacol. *144*, 466–473.

33. Chen, W.-H., Luo, G.-F., Qiu, W.-X., Lei, Q., Liu, L.-H., Wang, S.-B., and Zhang, X.Z. (2017). Mesoporous silica-based versatile theranostic nanoplatform constructed by layer-by-layer assembly for excellent photodynamic/chemo therapy. Biomaterials *117*, 54–65.

34. Luo, G.-F., Chen, W.-H., Lei, Q., Qiu, W.-X., Liu, Yu.-X., Cheng, Y.-J., and Zhang, X.-Z. (2016). A triple-collaborative strategy for high-performance tumor therapy by multifunctional mesoporous silica-coated gold nanorods. Adv. Funct. Mater. *26*, 4339–4350.

35. Bannasch, P. (2012). Glycogenotic hepatocellular carcinoma with glycogen-ground-glass hepatocytes: a heuristically highly relevant phenotype. World J. Gastroenterol. *18*, 6701–6708.

36. Bidkhori, G., Benfeitas, R., Klevstig, M., Zhang, C., Nielsen, J., Uhlen, M., Boren, J., and Mardinoglu, A. (2018). Metabolic network-based stratification of hepatocellular carcinoma reveals three distinct tumor subtypes. Proc. Natl. Acad. Sci. USA *115*, E11874–E11883.

37. McLoughlin, M.R., Orlicky, D.J., Prigge, J.R., Krishna, P., Talago, E.A., Cavigli, I.R., Eriksson, S., Miller, C.G., Kundert, J.A., Sayin, V.I., et al. (2019). TrxR1, Gsr, and oxidative stress determine hepatocellular carcinoma malignancy. Proc. Natl. Acad. Sci. USA *116*, 11408–11417.

38. Utreja, P., Jain, S., and Tiwary, A.K. (2012). Evaluation of biosafety and intracellular uptake of Cremophor EL free paclitaxel elastic liposomal formulation. Drug Deliv. *19*, 11–20.

39. Chen, W.-H., Liao, W.-C., Sohn, Y.-S., Fadeev, M., Cecconello, A., Nechushtai, R., and Willner, I. (2018). Stimul-responsive nucleic-acid –based polyacrylamide hydrogel-coated metal-organic ramework nanoparticles for controlled drug release. Adv. Funct. Mater. *28*, 1705137.

40. Dong, L., Zhou, H., Zhao, M., Gao, X., Liu, Y., Liu, D., Guo, W., Hu, H., Xie, Q., Fan, J., et al. (2018). Phosphorothioate-modified AP613-1 specifically targets GPC3 when used for hepatocellular carcinoma cell imaging. Mol. Ther. Nucleic Acids *13*, 376–386.

41. Dey, N.S., Mukherjee, B., Maji, R., and Satapathy, B.S. (2016). Development of linker-conjugated nanosize lipid vesicles: a strategy for cell selective treatment in breast cancer. Curr. Cancer Drug Targets *16*, 357–372.

42. Zhou, B.B., and Elledge, S.J. (2000). The DNA damage response: putting checkpoints in perspective. Nature *408*, 433–439.

43. Trinh, T.L., Zhu, G., Xiao, X., Puszyk, W., Sefah, K., Wu, Q., Tan, W., and Liu, C. (2015). A Synthetic aptamer-drug adduct for targeted liver cancer therapy. PLoS ONE *10*, e0136673.

44. Estève, M.A., Carré, M., and Braguer, D. (2007). Microtubules in apoptosis induction: are they necessary? Curr. Cancer Drug Targets *7*, 713–729.

45. Zhang, W., Hu, X., Shen, Q., and Xing, D. (2019). Mitochondria-specific drug release and reactive oxygen species burst induced by polyprodrug nanoreactors can enhance chemotherapy. Nat. Commun. *10*, 1704.

46. Ma, X., Gong, N., Zhong, L., Sun, J., and Liang, X.J. (2016). Future of nanotherapeutics: Targeting the cellular sub-organelles. Biomaterials *97*, 10–21.

47. Wang, H., Gao, Z., Liu, X., Agarwal, P., Zhao, S., Conroy, D.W., Ji, G., Yu, J., Jaroniec, C.P., Liu, Z., et al. (2018). Targeted production of reactive oxygen species in mitochondria to overcome cancer drug resistance. Nat. Commun. *9*, 562.

48. Dong, J., Liu, B., and Zhu, R. (2016). Targeting ROS for cancer therapy. Chemo. Open Access *5*, 1–7.

49. Baskić, D., Popović, S., Ristić, P., and Arsenijević, N.N. (2006). Analysis of cycloheximide-induced apoptosis in human leukocytes: fluorescence microscopy using annexin V/propidium iodide versus acridin orange/ethidium bromide. Cell Biol. Int. *30*, 924–932.

50. Liu, K., Liu, P.C., Liu, R., and Wu, X. (2015). Dual AO/EB staining to detect apoptosis in osteosarcoma cells compared with flow cytometry. Med. Sci. Monit. Basic Res. *21*, 15–20.

51. Li, F., Lu, J., Liu, J., Liang, C., Wang, M., Wang, L., Li, D., Yao, H., Zhang, Q., Wen, J., et al. (2017). A water-soluble nucleolin aptamer-paclitaxel conjugate for tumor-specific targeting in ovarian cancer. Nat. Commun. *8*, 1390.

52. Bates, P.J., Reyes-Reyes, E.M., Malik, M.T., Murphy, E.M., O'Toole, M.G., and Trent, J.O. (2017). G-quadruplex oligonucleotide AS1411 as a cancer-targeting agent: uses and mechanisms. Biochim. Biophys. Acta, Gen. Subj. *1861* (5 Pt B), 1414–1428.

53. Mulik, R.S., Mönkkönen, J., Juvonen, R.O., Mahadik, K.R., and Paradkar, A.R. (2010). Transferrin mediated solid lipid nanoparticles containing curcumin: enhanced in vitro anticancer activity by induction of apoptosis. Int. J. Pharm. *398*, 190–203.

54. Nakagawa, H., Hirata, Y., Takeda, K., Hayakawa, Y., Sato, T., Kinoshita, H., Sakamoto, K., Nakata, W., Hikiba, Y., Omata, M., et al. (2011). Apoptosis signal-regulating kinase 1 inhibits hepatocarcinogenesis by controlling the tumor-suppressing function of stress-activated mitogen-activated protein kinase. Hepatology *54*, 185–195.

55. Bao, H., Liu, P., Jiang, K., Zhang, X., Xie, L., Wang, Z., and Gong, P. (2016). Huaier polysaccharide induces apoptosis in hepatocellular carcinoma cells through p38 MAPK. Oncol. Lett. *12*, 1058–1066.

56. Chauhan, R., and Lahiri, N. (2016). Tissue-and serum-associated biomarkers of hepatocellular carcinoma. Biomark. Cancer *8* (*Suppl 1*), 37–55.

57. Zhang, Y., Deng, Z.S., Liao, M.M., Wang, N., Zhang, X.Q., Yu, H.Y., and Zhang, Y.D. (2012). Tumor associated glycoprotein-72 is a novel marker for poor survival in hepatocellular carcinoma. Pathol. Oncol. Res. *18*, 911–916.

58. Wang, C., Zhang, Y., Guo, K., Wang, N., Jin, H., Liu, Y., and Qin, W. (2016). Heat shock proteins in hepatocellular carcinoma: Molecular mechanism and therapeutic potential. Int. J. Cancer *138*, 1824–1834.

59. Cui, Y., Xu, Q., Chow, P.K.-H., Wang, D., and Wang, C.-H. (2013). Transferrin-conjugated magnetic silica PLGA nanoparticles loaded with doxorubicin and paclitaxel for brain glioma treatment. Biomaterials *34*, 8511–8520.

60. Guo, J., Gao, X., Su, L., Xia, H., Gu, G., Pang, Z., Jiang, X., Yao, L., Chen, J., and Chen, H. (2011). Aptamer-functionalized PEG-PLGA nanoparticles for enhanced anti-glioma drug delivery. Biomaterials *32*, 8010–8020.

61. Bradford, M.M. (1976). A rapid and sensitive method for the quantitation of microgram quantities of protein utilizing the principle of protein-dye binding. Anal. Biochem. *72*, 248–254.

62. Mukherjee, B., Ghosh, S., Das, T., and Doloi, M. (2005). Characterization of insulin-like-growth factor II (IGF II) mRNA positive hepatic altered foci and IGF II expression in hepatocellular carcinoma during diethylnitrosamine-induced hepatocarcinogenesis in rats. J. Carcinog. *4*, 12.

63. Ghosh, M.K., Patra, F., Ghosh, S., Hossain, C.M., and Mukherjee, B. (2014). Antisense oligonucleotides directed against insulin-like growth factor-II messenger ribonucleic acids delay the progress of rat hepatocarcinogenesis. J. Carcinog. *13*, 2.

64. Baghirova, S., Hughes, B.G., Hendzel, M.J., and Schulz, R. (2015). Sequential fractionation and isolation of subcellular proteins from tissue or cultured cells. MethodsX *2*, 440–445.

65. Dewanjee, S., Joardar, S., Bhattacharjee, N., Dua, T.K., Das, S., Kalita, J., and Manna, P. (2017). Edible leaf extract of *Ipomoea aquatica* Forssk. (Convolvulaceae) attenuates doxorubicin-induced liver injury via inhibiting oxidative impairment, MAPK activation and intrinsic pathway of apoptosis. Food Chem. Toxicol. *105*, 322–336.

66. Khanra, R., Bhattacharjee, N., Dua, T.K., Nandy, A., Saha, A., Kalita, J., Manna, P., and Dewanjee, S. (2017). Taraxerol, a pentacyclic triterpenoid, from *Abroma augusta* leaf attenuates diabetic nephropathy in type 2 diabetic rats. Biomed. Pharmacother. *94*, 726–741.

67. Hassan, N.M., Alhossary, A.A., Mu, Y., and Kwoh, C.K. (2017). Protein-ligand blind docking using QuickVina-W with inter-process spatio-temporal integration. Sci. Rep. *7*, 15451.

68. Yan, Y., Zhang, D., Zhou, P., Li, B., and Huang, S.Y. (2017). HDOCK: a web server for protein-protein and protein-DNA/RNA docking based on a hybrid strategy. Nucleic Acids Res. *45* (W1), W365–W373.

OMTN, Volume *20*

Supplemental Information

Aptamer-Functionalized Drug Nanocarrier Improves Hepatocellular Carcinoma toward Normal by Targeting Neoplastic Hepatocytes

Samrat Chakraborty, Zewdu Yilma Dlie, Somdyuti Chakraborty, Somdatta Roy, Biswajit Mukherjee, Shila Elizabeth Besra, Saikat Dewanjee, Alankar Mukherjee, Probir Kumar Ojha, Vinay Kumar, and Ramkrishna Sen

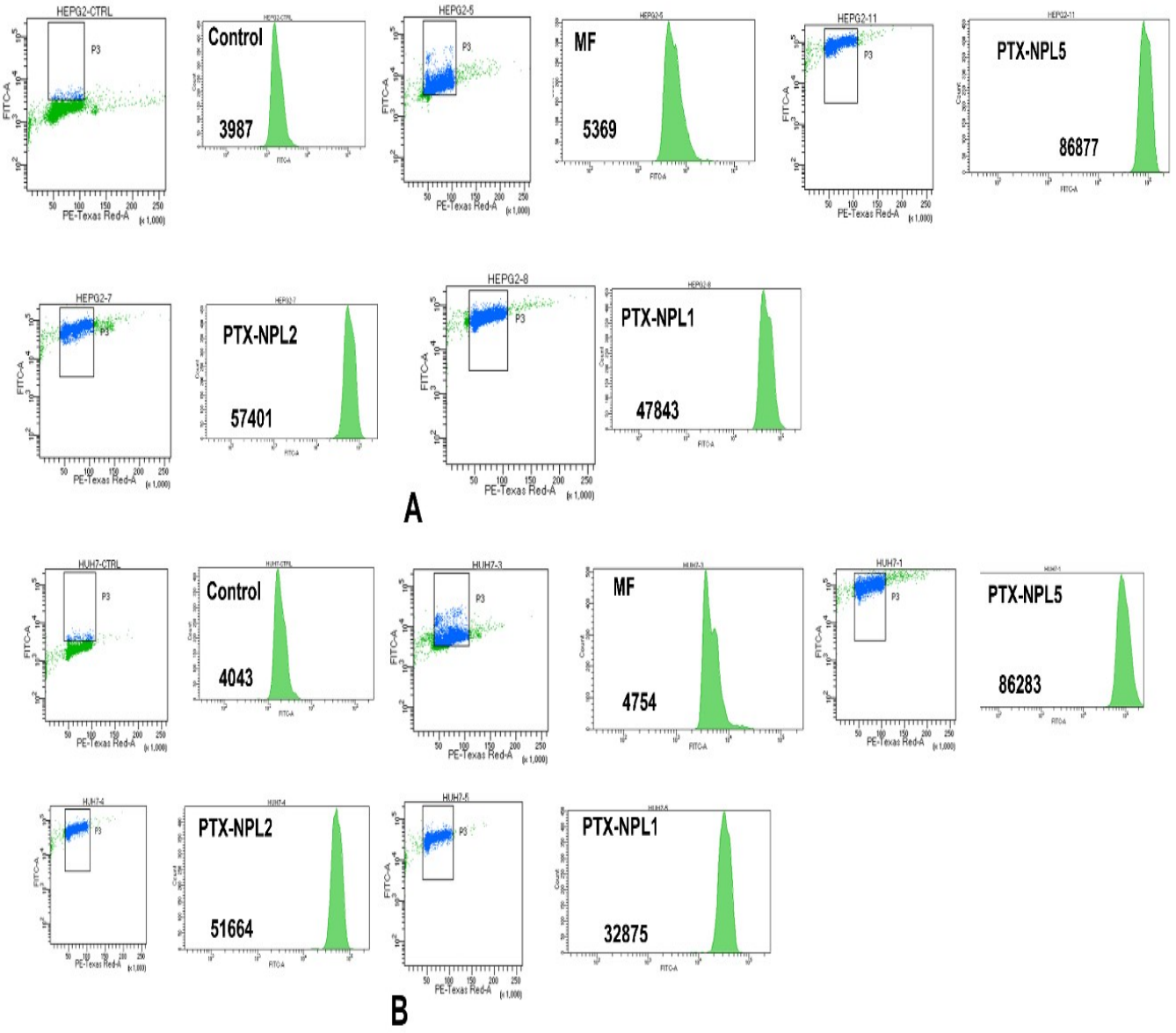

Figure S1 Quantitative determination of extent of DNA fragmentations measured by Apo-BrdU DNA fragmentation assay kit (A) in HepG2 and (B) in Huh-7 cells respectively upon treatment with MF/PTX-NPL5/PTX-NPL2/PTX-NPL1. Numbers in each block denotes the levels of fluorescent signals. Control cells depicts cells without treatment and various treatments are shown for cells treated with various experimental formulations as mentioned in each block. Rise in fluorescent signal directly proportional to DNA strand-breaks which in turn signify DNA fragmentation.

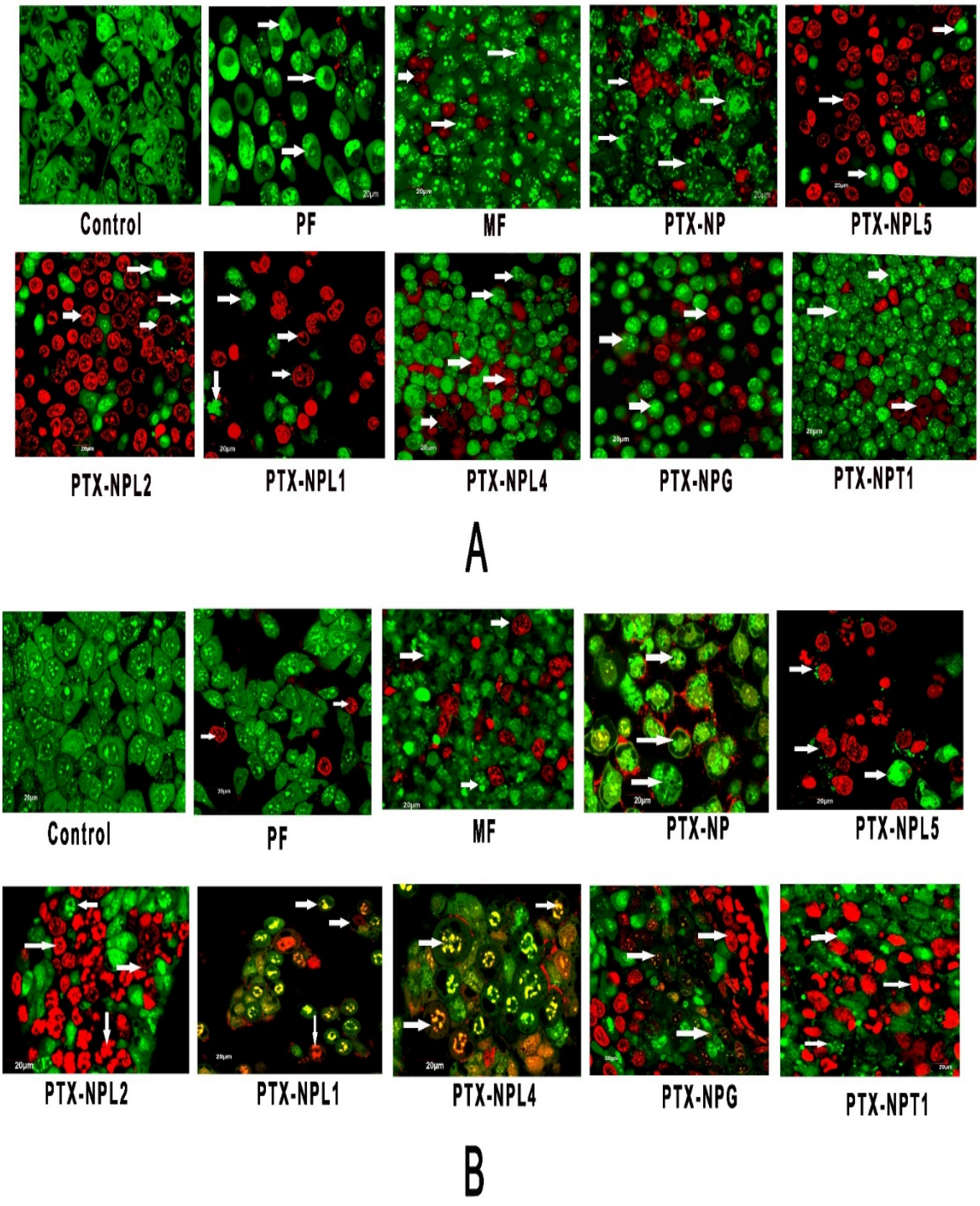

Figure S2 Morphological changes in (A) HepG2 cells and (B) Huh-7 cells respectively, treated with different treatments as mentioned under each image. Cells without treatment considered as control. Morphological changes are indicated by arrowheads. (Scale bar - 20µm)

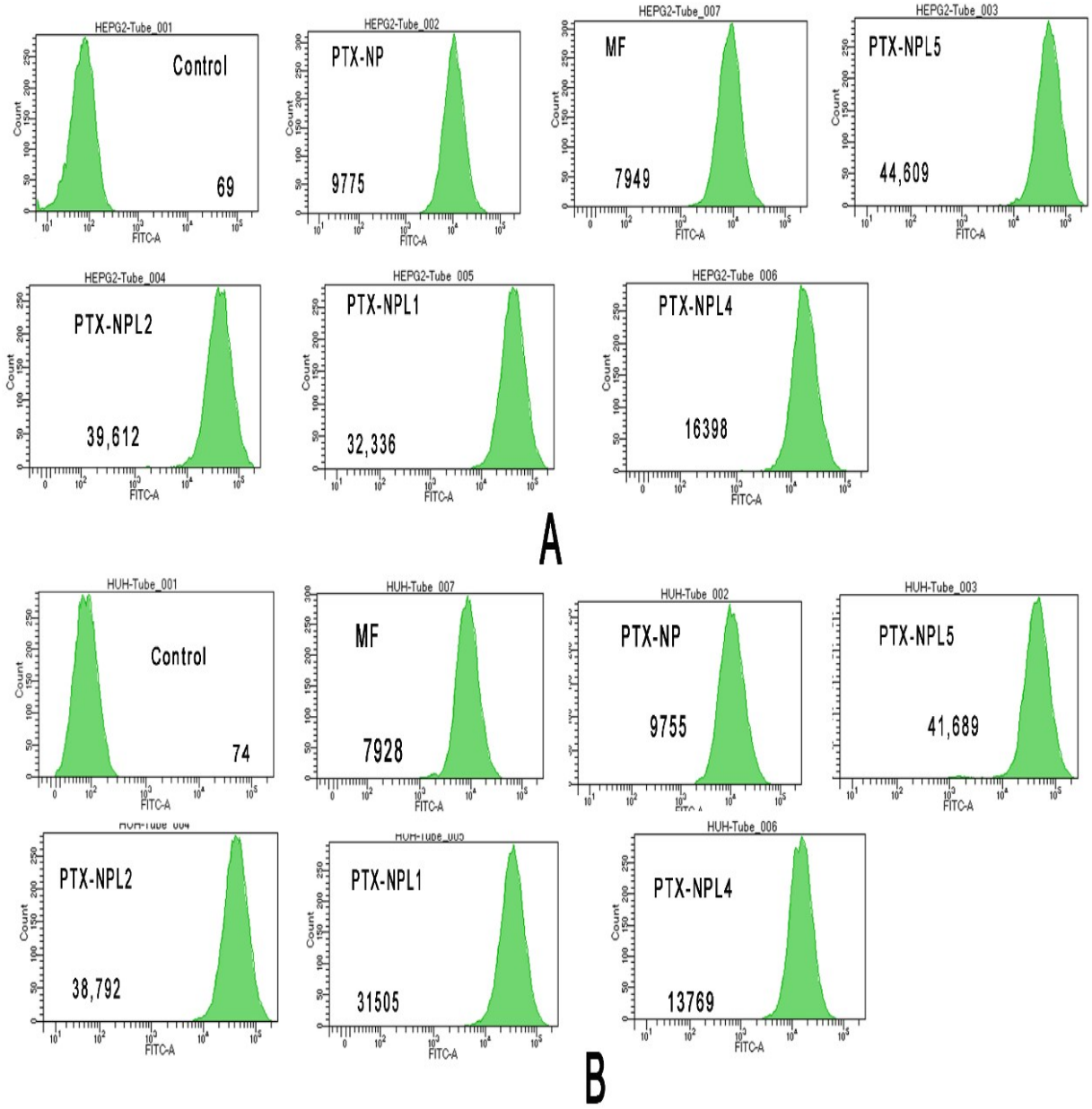

Figure S3 Levels of reactive oxygen species (ROS) (as denoted by numbers), (A) in HepG2 and (B) in Huh7 cells upon treatment with different experimental formulations as mentioned in each block. Cells without treatment considered as control.

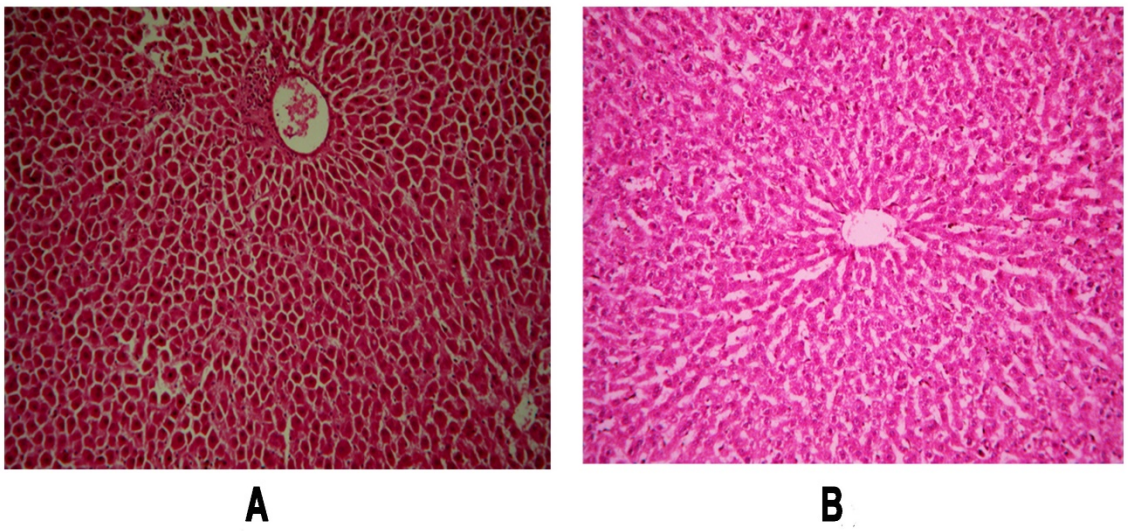

Figure S4 Histopatological examination of liver of normal rats upon treatment with PTX-NPL5. A. Image of liver of normal (control) rats, at 100 X magnification upon H&E staining B. image of liver of normal rats at 28^{th} day upon treatment with PTX-NPL5, at 100 X magnification upon H&E staining. No distinctive changes in liver architecture was observed, indicating its extremely low or no-toxicity against normal hepatocytes.

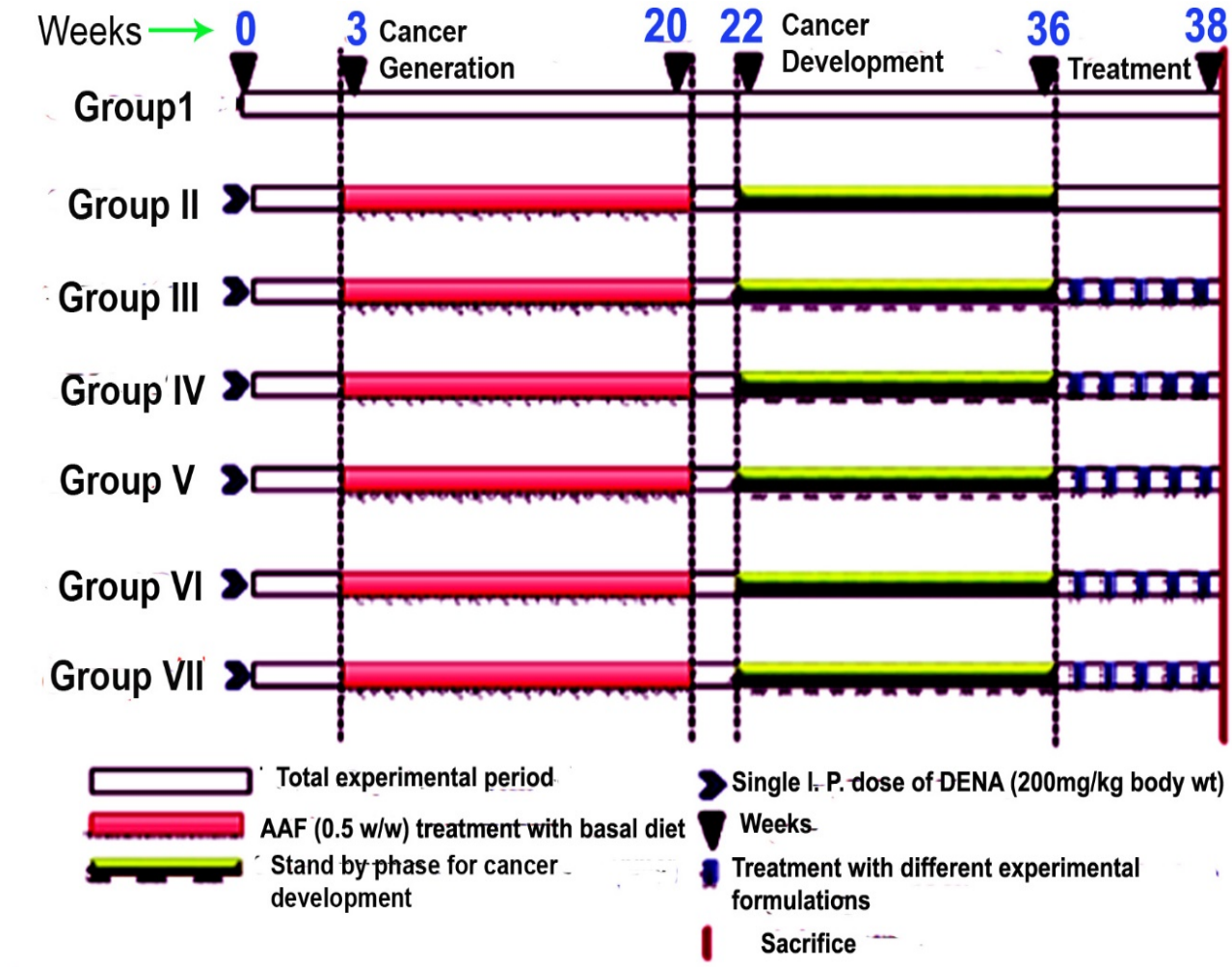

Figure S5 Scheme for induction of chemically-induced hepatocarcinogenesis in rats. Group-I (normal control rats), Group-II (carcinogen control rats), Group-III (carcinogen treated rats received MF), Group-IV (Carcinogen treated rats received PTX-NPL5), Group –V(carcinogen treated rats received PTX-NP), Group VI (carcinogen treated rats received PTX-NPL2), Group VII(carcinogen treated rats received PF)

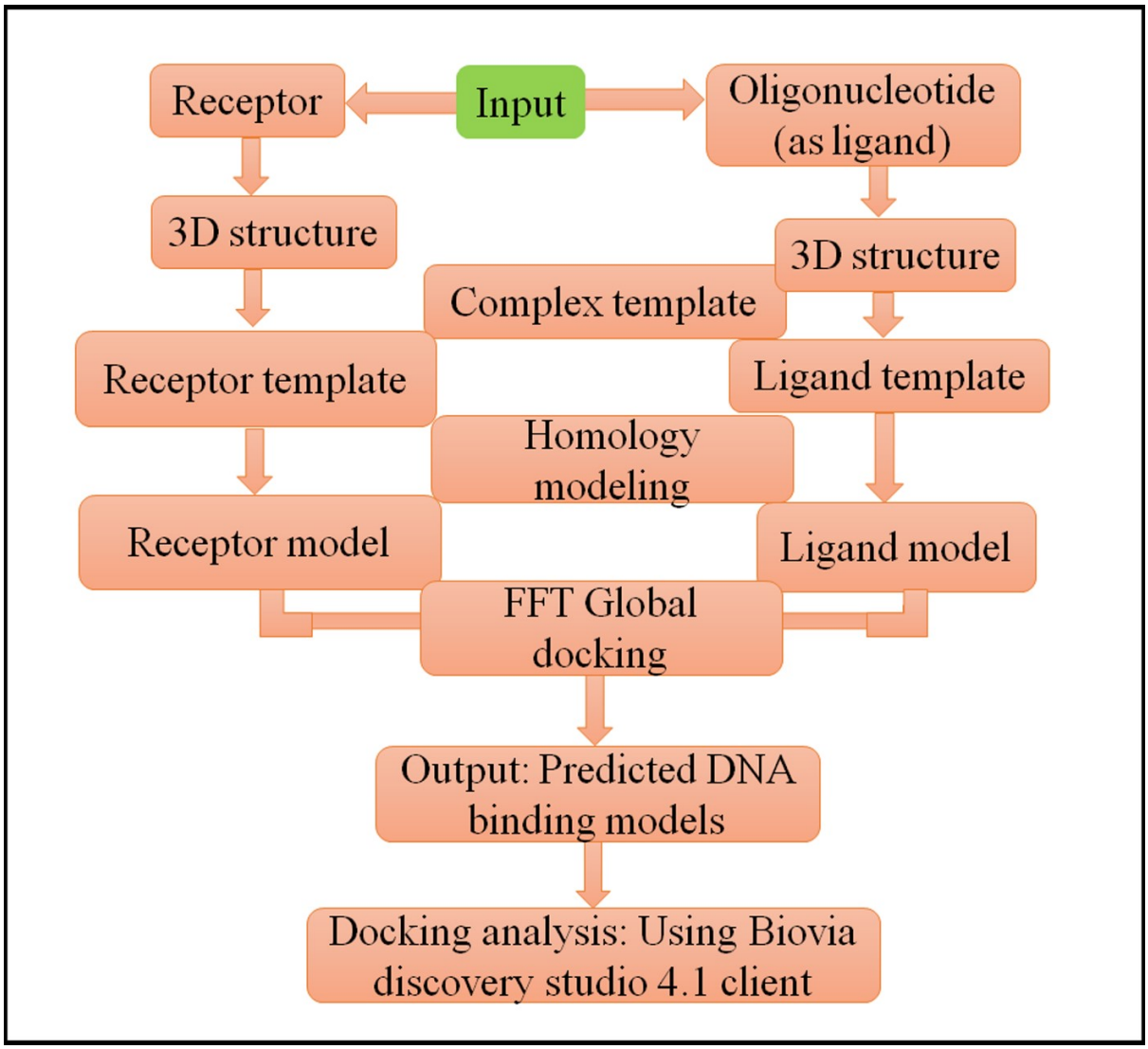

Figure S6 Schematic representation of blind docking protocol to analyse ligand-receptor interaction of L2 and L5

Table S1 Physical characterizations of experimental nanoparticles

Name of the formulation	Average particle diameter (Z-average) (nm)	Polydispersity index	Zeta potential (mV)	Drug-loading (%)	Entrapment efficiency (%)
PTX-NP	181.5± 12.25	0.334	-10.7± 4.27	5.98±0.55	65.78±4.04
PTX-NPL1	217.9± 8.04	0.246	-15.0± 5.27	6.31±0.46	69.41± 1.65
PTX-NPL2	236.1±17.34	0.532	-17.7± 5.19	6.38±0.63	70.18±2.14
PTX-NPL3	229.6±15.44	0.459	-17.2± 3.16	6.05±0.43	66.55 ±2.07
PTX-NPL4	220.2± 18.25	0.323	-16.3±3.71	6.14±0.37	67.54±4.18
PTX-NPL5	211.9±13.43	0.285	15.6± 4.06	6.45± 0.45	70.95±3.69
PTX-NPG	240.9±17.09	0.356	-14.6± 3.71	6.35±0.62	69.85± 2.76
PTX-NPT1	242.4±19.67	0.329	-13.0±5.46	6.23±0.53	68.53±3.19

[a]Data show mean ± SD (n=3)

Table S2 IC_{50} doses and % inhibition in various cancerous and normal cell types, upon the treatment of experimental formulations, free-drug suspension (PF) and commercial formulation (MF)

Treatment Groups	IC_{50} dose in HepG2 cells (nM)	IC_{50}dose in Huh-7 cells (nM)[a]	% inhibition in Chang liver cells[a]	% inhibition in WRL-68 cell
PF	995.76 ± 3.2 [a]	989.16 ± 6.43	63.41 ± 5.88 [a]	64.51± 4.08
PTX-NP	194.71 ± 6.23	198.01 ± 4.45	8.57 ± 2.50	8.89 ± 3.50
PTX-NPL1	73.61 ± 5.68	75.48 ± 3.84	9.25 ± 2.75	9.83 ± 2.28
PTX-NPL2	64.54 ± 5.21	67.82 ± 6.34	9.65 ± 3.68	9.7 ± 4.91
PTX-NPL3	192.61 ± 5.71	194.28 ± 5.45	8.62 ± 3.59	8.72 ± 2.75
PTX-NPL4	95.06 ± 5.48	98.27 ± 5.86	9.82 ± 3.94	9.58 ± 3.73
PTX-NPL5	42.87 ± 2.56	46.64 ± 6.48	8.04 ± 2.44	8.36 ± 2.91
PTX-NPT1	175.56 ± 5.68	178.19 ± 5.36	19.64 ± 4.61	19.2 ± 2.4
PTX-NPG	147.23 ± 6.45	152.99 ± 6.43	18.21 ± 3.1	19.81 ± 2.33
MF	380.06 ± 5.83	363.51± 4.51	71.85 ± 6.56	74.45 ± 3.98

[a]Data show mean ± standard deviation (n=3)

Table S3 Tumor incidences, numbers and size distribution of hepatic altered foci (HAF) and area of neoplastic lesions on rats-treated with hepatocarcinogen (carcinogen control rats) and carcinogen-treated rats treated with different experimental formulations

Groups	Numbers of tumor bearing rats/ total no. of rats	Size distribution of HAF (% of total no.)			Area of lesion (% of total hepatic area observed)
		<1mm	>1mm to <3mm	> 3mm	
Normal control rats	0/6	00	00	00	00
Carcinogen-control rats	6/6	16.07±1.16	40.65±.098	43.51±3.12	HAF = 83.23±3.02[a]
Carcinogen-treated rats treated with free-drug (PF)	6/6	16.38±1.32	41.01±1.15	42.61±2.67	HAF= 82.04±3.21
Carcinogen-treated rats treated with commercial (MF)	5/6	13.19±1.06*	48.53±2.27	38.28±2.19	HAF = 71.62±4.18
Carcinogen-treated rats treated with PTX-NP	4/6	32.45±3.62*	42.39±4.21*	25.14±4.01*	HAF= 52.43±2.33
Carcinogen-treated rats treated with PTX-NPL2	2/6	58.45±4.21*	26.87±3.86*	14.68±3.06*	HAF = 31.45±2.85
Carcinogen-control rats – treated with PTX-NPL5	0/6	82.47±3.48*	14.56±4.5*	3.08±0.056*	HAF = 19.23±3.53

Data show mean ± SD (n=6). "*" indicates $p<0.05$ when compared with data of carcinogen-control rats.

Table S4 Determination of body weight of rats belong to different to different groups used for in vivo study during the course of the experiment

Days/weeks	Normal-control Rats	Carcinogen-control rats	Carcinogen-treated rats treated with free-drug suspension (PF)	Carcinogen-treated rats treated with commercial formulation (MF)	Carcinogen-treated rats treated with PTX-NP	Carcinogen-treated rats treated with PTX-NPL2	Carcinogen-treated rats treated with PTX-NPL5
1st Day	141.2± 5.2[a, b]	144.4 ± 7.5	143.4 ± 6.8 [a, b]	148.7 ± 5.4	147.5 ± 4.6	146.6 ± 4.3	140.4 ± 5.8
7th day (1st week)	145.8 ± 6.3	143.7 ± 6.3	141.8 ± 9.2	146.5 ± 4.9	144.4 ± 6.6	144.4 ± 5.2	141.01 ± 4.7
2nd week	148.5 ± 6.5	142.4± 6.3	141.9 ± 3.9	145.2 ± 5.6	140.6 ± 3.7	142.2 ± 6.3	139.6 ± 5.2
3rd week	152.3 ± 4.6	140.8 ± 7.5*	139.7 ± 5.3*	144.4 ± 3.8*	139.1 ± 5.2*	140.7 ± 8.3*	140.2 ± 7.5*
4th week (First month)	156.4 ± 5.5	139.8 ± 4.8*	138.6 ± 6.4*	145.8 ± 5.3*	138.4 ± 3.5*	138.9 ± 6.2*	138.7 ± 8.1*
5th week	162.8 ± 6.3	138.5 ± 5.8*	138.1± 4.6*	143.9 ± 5.8*	137.6 ± 4.4*	136.6 ± 5.3*	137.2 ± 4.1*
6th week	170.4 ± 6.2	136.6 ± 5.9*	137.8 ± 3.6 *	142.3 ± 6.4*	136.8 ± 5.3*	136.5 ± 4.5*	136.8 ± 7.1*
7th week	178.6 ± 8.2	134.4 ± 10.2*	136.2 ± 5.8*	139.8 ± 4.4*	134.4 ± 5.2*	135.3 ± 7.8*	134.8 ± 3.4*
8th week (2nd Month)	186.4 ± 9.2	130.5 ± 5.5*	132.7 ± 8.6*	135.8 ± 6.8*	129.8 ± 4.8*	130.5 ± 5.6*	131.8 ± 6.5*
Third month	196 ± 5.8	127.3 ± 5.8*	129.8 ± 6.4*	128.8 ± 3.6*	126.6 ± 5.5*	127.8 ± 6.2*	128.6 ± *4.6
Fourth month	204.6 ± 5.7	125.8 ± 4.3*	126.4 ± 4.6	125.6 ± 4.8*	124.6 ± 6.4*	124.4 ± 5.1*	125.1 ± 3.7*
Fifth Month	212.3 ± 6.9	123.4 ± 5.8*	123.6 ± 5.8*	122.2 ± 5.8*	122.6 ± 7.4*	121.8 ± 4.8*	122.4 ± 6.5*
Sixth Month	220 ± 9.8	120.6 ± 5.8*	121.8 ± 5.8*	120.4 ± 8.2*	119.7 ± 5.1*	119.6 ± 7.4*	118.4 ± 4.8*
Seventh Month	225.7 ± 9.5	117.6± 5.8*	118.8 ± 4.7*	116.8 ± 7.6*	116.7 ± 5.8*	115.4 ± 5.2*	114.8 ± 3.6*
Eight month	229.6 ± 8.8	114.7 ± 4.5*	112.7± 4.7*	113.4 ± 5.5*	113.8 ± 4.8*	111.6 ± 5.6*	110.7 ± 4.4*
Nine month	235.6 ± 10.52	109.6 ± 3.5*	108.8 ± 5.3*	108.9 ± 6.2*	107.5 ± 4.2*	107.8 ± 3.3*	105.4 ± 5.1*
After treatment							
One day			110.4 ± 5.4	110.7 ± 5.8	112.3 ± 4.8	113.4 ± 3.7	111.3 ± 4.8
3rd day			111.4 ± 4.1	116.9 ± 4.7	117.1 ± 7.5	119.6 ± 8.4	120.8 ± 5.8
7th day			113.8 ± 3.2	118.6 ± 3.9#	122.4 ± 4.3#	125.6 ± 5.1#	126.8 ± 2.6#

10th Day	113.6 ± 6.8	119.8 ± 5.8#	130.6 ± 4.5#	133.6 ± 4.8#	134.8± 5.4#
14th Day	112.4 ± 7.2	118.8 ± 4.6#	132.8 ± 8.6#	136.6 ± 6.4#	139.8 ± 3.7#

[a]weight of the rats were expressed in gram, [b]data are expressed as mean ±SD (n=6). "*" indicates $p < 0.05$ when the weights of rats belong to carcinogen-control group and different treatments groups were compared withthe rats of normal control group before the treatment. "#" indicates $p < 0.05$ when the weights of rats of different treatments groups were compared with those of the rats carcinogen-control group.

Table S5 Levels of different biochemical parameters in liver of normal rats treated with different treatments

Group	SGPT (IU/l) ±SD(n=3)		SGOT (IU/l) ±SD(n=3)		ALK (IU/l) ±SD(n=3)	
	0 days	28 days	0 days	28 days	0 days	28 days
Control	43.73 ±1.51[a]	46.85 ±1.45	58.77±2.81	60.61± 2.09	191.32± 2.70	213.58± 1.57
PF	47.37±1.64*	64.03 ±1.59*	61.16±2.42	96.50± 1.15*	196.62± 3.90*	252.29± 3.70*
MF	49.22 ±1.00*	95.68 ±3.94*	62.31± 1.08*	122.71± 2.71*	195.56± 4.15*	294.03± 3.55*
PTX-NP	41.27 ±1.01	57.43 ±1.02*	54.96± 3.88	75.30± 3.09*	194.89± 2.17*	225.99± 2.13*
PTX-NP L2	41.57 ±1.53	51.91± 1.16	56.66± 3.08	72.69± 3.71*	196.01± 2.93	227.11± 4.05*
PTX-NP L5	40.28 ±1.07	49.62± 1.46	55.24± 1.18	70.57± 1.70	192.10± 1.15	222.43± 3.92

[a] Data mean ± SD (n=6) ; "*"indicates $p<0.05$ with respect to the value of control group of rats

Table S6 Changes in bodyweight of normal rats–treated with different treatments

Days	Normal control rats	Normal control rats-treated with free-drug suspension (PF)	Normal control rats-treated with commercial formulation (MF)	Normal control rats-treated with PTX-NP	Normal control rats-treated with PTX-NPL2	Normal control rats-treated with PTX-NPL5
1st Day	140.5 ± 5.4[a, b]	139.8 ± 4.5[a, b]	141.4 ± 3.6	142.3 ±6.2	145 ± 6.5	143± 5.8
2nd Day	140.8 ± 4.8	135.2 ± 5.2*	129.8 ± 4.4*	140± 5.6	143 ±4.8	142± 3.5
3rd Day	141.4 ± 4.4	126.5 ± 3.4*	117.6 ±5.9*	138.6 ± 4.8	142 ±5.1	140 ± 3.8
4TH day	143.6 ± 6.4	115 ± 7.6*	102.6 ± 4.8*	137.4 ± 5.5	140.8 ±2.8	139.4 ± 4.4
7th day	144.8 ± 4.5	108 ± 5.6*	90.5 ± 5.4*	138.5 ±3.2	141.5 ± 4.8	140.4 ± 6.6
14th day	146.2 ± 6.5	98.9 ± 4.4*	75.3 ± 3.8*	137.4 ±5.8	140.4 ± 6.4	140.8 ±3.6
21st day	147.8 ± 5.8	90.5 ± 6.3*	62.5 ± 4.5*	138.7 ±2.8	141.3 ±5.7	141.4 ±5.4
28th day	149.2 ±4.3	79.7 ± 2.6*	48.7 ± 6.4*	137.3 ± 5.5	139.8 ± 4.2	140.6 ±4.3

[a] weight of rats were expressed in gram, [b]data were expressed as mean ± SD (n=6). Statistical level of significance is indicated as "*"($p<0.05$), when the data of the treatment groups were compared with those of the normal (control) rats.

Table S7: Concentration of PTX (ng/g liver) in normal SD rats upon i.v. administration of experimental formulations

Time (h)	Upon administration of free-drug (PF)	Upon administration of commercial formulation (MF)	Upon administration of PTX-NP	Upon administration of PTX-NPL2	Upon administration of PTX-NPL5
1	97.17 ± 2.34[*]	230.16 ± 8.21[c]	116.12± 2.56[b,e]	120.45± 3.28[c,e]	118.24± 4.45[b,e]
2	219.45 ± 4.13	328.12 ± 2.19[c]	198.12± 6.28[b,e]	203.34± 3.48[a,e]	201.24± 6.67[b,e]
4	267.71± 9.82	431.25 ± 7.73[c]	231.19± 4.21[c,e]	235.72± 2.17[c,e]	233.57± 5.13[c,e]
6	92.74 ± 7.48	418. 25 ± 5.45[c]	320.16± 4.13[c,e]	322.68± 5.32[c,e]	325.48± 2.26[c,e]
8	18.83 ± 3.86	226.27 ± 4.32[c]	202.37± 2.62[c,e]	205.81± 4.18[c,e]	208.41± 3.19[c,d]
10	BLQ	130.48 ± 6.18	104.16± 5.13	106.38 ± 3.18	108.51± 4.82
24	BLQ	56.57 ± 3.28	44.82 ± 7.32	46.58 ± 8.23	42.34 ± 5.21
48	BLQ	26.12 ± 4.38	14.47 ± 5.29[d]	15.65 ± 4.15[d]	13.46 ± 7.14[d]

[*]Data show mean ± SD (n=3). [(a,b,c,d,e)]Significant difference when compared to the data obtained upon free-drug treatment ([a]$p<0.05$, [b]$p<0.01$, [c]$p<0.001$), commercial formulation treatment ([d]$p<0.01$, [e]$p<0.001$).

BLQ denotes below the quantification limit (<2ng/ml)

Table S8: Concentration of PTX (ng/g of liver) in carcinogen-treated SD rats upon i.v. administration of experimental formulations.

Time (h)	Upon administration of free-drug (PF)	Upon administration of commercial formulation (MF)	Upon administration of PTX-NP	Upon administration of PTX-NPL2	Upon administration of PTX-NPL5
1	94.26 ± 4.12*	141.82 ± 3.58[a]	169.41± 5.14[a,b]	234.13 ± 4.17[a,b,c]	249.42 ± 5.35[a,b,c]
2	215.61 ± 5.32	342.56 ± 5.16[a]	239.71± 4.22[a,b]	398.41± 4.23[a,b,c]	418.12 ± 5.28[a,b,c]
4	261.84± 3.59	451.78 ± 3.74[a]	272.56± 3.39[a,b]	528.81± 7.24[a,b,c]	563.19 ± 3.20[a,b,c]
6	96.88± 4.84	429.17 ± 4.77[a]	471.91± 7.87[a,b]	702.76± 3.36[a,b,c]	728.26 ± 4.69[a,b,c]
8	32.18± 6.71	232.61 ± 5.16[a]	335.63±3.38[a,b]	615.57± 7.20[a,b,c]	641.56 ± 7.89[a,b,c]
10	11.78 ± 5.43	145.27 ± 2.29[a]	153.69± 4.27[a,b]	414.53± 5.49[a,b,c]	436.18 ± 6.43[a,b,c]
24	4.12 ± 1.68	66.41 ± 4.52[a]	107.18± 6.17[a,b]	245.26± 5.23[a,b,c]	268.93 ± 4.87[a,b,c]
48	BLQ	12.62 ± 9.12	51.29± 2.28[a,b]	132.65 ± 4.15[a,b,c]	156.45 ± 2.97[a,b,c]

*Data show mean ± SD (n=3). [(a,b,c)]Significant difference when compared to the data obtained upon free-drug treatment ([a]$p<0.01$), commercial formulation treatment ([b]$p<0.01$) and PTX-NP treatment ([c]$p<0.01$).

BLQ denotes below the quantification limit (<2ng/ml)

Table S9 Docking results of 39 and 63 base pair oligonucleotides with surface biomarker proteins of neoplastic hepatocytes.

S. No	Name of Protein	PDB ID	(-) Docking Score	Interacting Residues	Interactions
			Oligonucleotide with 39 base pairs		
1	Tumor Associated Glycoprotein 72 (TAG-72)	6bsb	227.82	ALA: 1106, PHE: 1042, LEU: 1089, THR: 1104, PHE: 1146, ASN: 1091, ASP: 1143, SER: 1142, PHE: 1044, SER: 1137, ASP: 1138, HIS: 1138, GLU: 1118, ASN: 1122 and LYS: 1125	Hydrogen bonding (classical and non-classical) interactions, Salt bridge, Attractive charges, π-Anion, π-π-T-shaped, π-πstacked and π-sigma and π-alkyl
2	Heat shock protein-70 (HSP- 70)	6do2	235.68	LYS: 163, THR: 29, LYS: 46, ASN: 47, GLY: 407, LEU: 405, ASP: 26, VAL: 27, MET: 196, ARG: 49, GLY: 40, GLU: 51, TYR: 160, SER: 406, LYS: 185, ILE: 199, ILE: 198, ARG: 197, LYS: 213, GLY: 240	Hydrogen bonding (classical and non-classical) interactions, Salt bridge, attractive charges, π-π stacked, π-alkyl, π-sigma
			Oligonucleotide with 63 base pairs		
1	Tumor Associated Glycoprotein 72 (TAG-72)	6bsb	205.23	HIS: 1048, ASP: 1138, SER: 1140, SER: 1046, GLN: 1102, SER: 1074, ASN: 1091, GLY: 1088, LEU: 1087, ARG: 1108, PHE: 1044, SER: 1142, VAL: 1144 and PHE: 1146	Hydrogen bonding (classical and non-classical) interactions, Attractive charges, π-π-T shaped, π-πstacked, π-sigma

2	Heat shock protein-70 (HSP- 70)	6do2	230.46	MET: 196, VAL: 27, ASP: 26, GLY: 407, ASN: 47, LYS: 46, TYR: 160, GLU: 51, LYS: 46, ARG: 49, SER: 406, THR: 29, GLN: 401, ILE: 207, LYS: 163, ILE: 198, ILE: 199, ARG: 197, GLY: 204LYS: 213, LYS: 185	Hydrogen bonding (classical and non-classical) interactions, Salt bridge, attractive charges, π-cation, π-πstacked, π-alkyl, π-sigma, π-Sulphur